

Supporting Information

Dysprosium-dianthracene framework showing thermo-responsive magnetic and luminescent properties

Qian Zou,^a Tao Shang,^b Xin-Da Huang,^a Qing-Qing Guo,^a Jia-Ge Jia,^a Song-Song Bao,^{*a} Yi-Quan Zhang^{*b} and Li-Min Zheng^{*a}

Content

Table S1. A list of Dy-MOFs showing slow magnetization relaxation.....	S2
I. Primary characterization	S4
II. Crystal structures	S6
III. Sorption properties	S9
IV. Thermo-induced phase transitions	S11
V. Optical properties	S14
VI. Magnetic studies	S22
VII. Magnetic computational details	S32

Table S1. A list of Dy-MOFs showing slow magnetization relaxation.

Compounds formula	Space group	Quasi-coordination symmetry	H_{dc} (kOe)	U_{eff} (K)	τ_0 (s)	Ref.
[Dy(TDA) _{1.5} (H ₂ O) ₂] _n	<i>C</i> 2/ <i>c</i>	<i>C</i> _{2v}	0	44.2	2.4×10 ⁻⁸	1
{[Dy ₂ Zn(BPDC) ₃ (H ₂ O) ₄](ClO ₄) ₂ } _n	<i>C</i> 2/ <i>c</i>	<i>D</i> _{3h}	5	90.9	3.84×10 ⁻¹⁰	2
[DyCu(BPDC) ₂ (H ₂ O) ₂ Cl] _n	<i>C</i> 2/ <i>c</i>	<i>C</i> _{2v}	2	42.4	3.43×10 ⁻⁹	3
{[Dy ₂ Cu(BPDC) ₃ (H ₂ O) ₄](NO ₃) ₂ } _n	<i>C</i> 2/ <i>c</i>	<i>D</i> _{3h}	5	95.3	9.4×10 ⁻¹¹	3
[Dy(BTC)] _n	<i>P</i> 4 ₃ 22	<i>D</i> _{3h}	1	45.9	2.43×10 ⁻⁶	4
{KDy(ox) ₂ (H ₂ O) ₄ } _n	<i>I</i> 4 ₁ / <i>amd</i>	<i>D</i> _{4d}	0	417	1.23×10 ⁻⁹	5
{KDy(ox) ₂ } _n	n.a.	<i>D</i> _{4d}	0	418	3.0×10 ⁻⁹	5
{[Dy(bipyNO) ₄](TfO) ₃ } _n	<i>P</i> 1̄	<i>D</i> _{4d}	1	17.9	1.86×10 ⁻⁷	6
{[Na ₄ Dy ₁₂ (stp) ₈ (OH) ₁₆ (H ₂ O) ₁₂]·10H ₂ O} _n	<i>C</i> 2/ <i>m</i>	<i>D</i> _{4d}	0	13.7	8.82×10 ⁻⁷	7
[Dy(phen)(L ¹)] _n	<i>P</i> 2 ₁ / <i>n</i>	<i>D</i> _{5h}	0	131	1.6×10 ⁻⁶	8
(EMIM)[Dy ₃ (BDC) ₅]	<i>P</i> 2 ₁ / <i>c</i>	<i>D</i> _{2d} , <i>C</i> _{4v} , <i>D</i> _{3h}	2	39.3	2.6×10 ⁻¹⁰	9
[DyCd ₂ (PIDC)(HPIDC)(H ₂ O) ₅ Cl ₂] _n	<i>C</i> _c	<i>D</i> _{4d}	1.4	53	1.86×10 ⁻⁸	10
[Dy ₂ (FDA) ₃ (DMF) ₂ ·1.5DMF] _n	<i>C</i> 2/ <i>c</i>	<i>C</i> _{2v}	2	41.8	1.08×10 ⁻⁸	11
[Dy ₂ (FDA) ₃ (DMF) ₂ (MeOH) ₂] _n	<i>C</i> 2/ <i>c</i>	<i>C</i> _{2v}	2	67.5	2.26×10 ⁻¹¹	11
{[Dy ₂ (INO) ₄ (NO ₃) ₂]·2DMF} _n	<i>P</i> 2 ₁ / <i>c</i>	<i>C</i> _{4v}	0	n.a.	n.a.	12
{[Dy ₂ (INO) ₄ (NO ₃) ₂]·2MeCN} _n	<i>P</i> 2 ₁ / <i>c</i>	<i>C</i> _{4v}	0	110	3.24×10 ⁻¹¹	12
[[Dy ₂ (1H-5-Cl-6-Opy-3-CO ₂) ₂ (ox) ₂ (H ₂ O)]·2H ₂ O] _n	<i>P</i> nma	<i>C</i> _{4v} , <i>D</i> _{5h}	2	37.6	3.5×10 ⁻⁶	13
[[Dy(hfac) ₃] ₂ (bpdo) ₂] _n	<i>F</i> 2dd	<i>C</i> _{4v}	1.9	10.3	1.25×10 ⁻⁵	14
{[Dy(ant) _{1.5} (DMF) ₂]·(DMF)} _n	<i>P</i> 1̄	n.a.	1	52.7	2.7×10 ⁻⁷	15
{[Dy((NH ₂) ₂ -bdc) _{1.5} (DMF) ₂]·DMF·H ₂ O} _n	<i>P</i> 1̄	<i>D</i> _{4d}	1	32	6.17×10 ⁻⁸	16
{[Dy ₂ (μ ₄ -CNip)(μ ₃ -CNip) ₂ (DMF) ₄]·DMF·H ₂ O} _n	<i>Ī</i> 42d	<i>D</i> _{4d}	0	44	1.5×10 ⁻⁷	17
{[Dy(C ₂ O ₄) _{1.5} phen]·0.5H ₂ O} _n	<i>C</i> 2/ <i>c</i>	<i>D</i> _{4d}	1.2	35.5, 32.6	3.1×10 ⁻¹⁰ , 1.0×10 ⁻⁹	18
[Dy(BTB)H ₂ O] _n	<i>F</i> ddd	<i>D</i> _{3h}	1	17.8	1.4×10 ⁻⁷	19
{[Dy(DMTDC) _{1.5} (H ₂ O) ₂]·0.5DMF·0.5H ₂ O} _n	<i>C</i> 2/ <i>c</i>	<i>C</i> _{2v}	2	48.3	4.38×10 ⁻⁷	20
[DyL ² (H ₂ O) ₃]·3H ₂ O·0.75DMF	<i>P</i> bcn	<i>D</i> _{2d}	1.2	57	3.89×10 ⁻⁸	21
[Dy(TATB)(DMF) ₂]	<i>C</i> 2/ <i>c</i>	<i>D</i> _{4d}	3	32.4	2.1×10 ⁻⁶	22
[Dy(<i>o</i> -PDA) ₃ (H ₂ O) ₂]·2H ₂ O] _n	<i>C</i> 2/ <i>c</i>	<i>C</i> _s	0	9.1	1.6×10 ⁻⁵	23
[Dy(Habtc)]·1.8H ₂ O	<i>P</i> 1̄	<i>D</i> _{2d}	1	n.a.	n.a.	24
{[Dy(L ³)(μ ₂ -bpdo) _{0.5} (μ ₄ -bpdo) _{0.5} (CH ₃ OH)]·ClO ₄ ·3CH ₃ OH} _n	<i>P</i> 1̄	<i>D</i> _{2d}	0	393	6.75×10 ⁻¹¹	25
{[Dy(L ³) (μ ₂ -bpdo) _{0.5} (μ ₄ -bpdo) _{0.5} (CH ₃ OH)]·ClO ₄ } _n	<i>P</i> 1̄	<i>D</i> _{2d}	0	348	1.15×10 ⁻¹⁰	25
[Dy ₂ Co(2,3-pzdc) ₄ (H ₂ O) ₄]·4H ₂ O	<i>P</i> 2 ₁ / <i>n</i>	<i>C</i> _{4v}	2	5	1×10 ⁻⁵	26
[Dy ₂ Cu(2,3-pzdc) ₄ (H ₂ O) ₄]·4H ₂ O	<i>P</i> 2 ₁ / <i>n</i>	<i>D</i> _{4d}	2	102.4	7.0×10 ⁻¹¹	26
{(Me ₂ NH ₂)[Dy(OBA) ₂](Hatz)(H ₂ O) _{1.5} } _n	<i>P</i> 6422	<i>D</i> _{2d}	1	15	4.4×10 ⁻⁷	27

[Dy(3,4'-oba)(phen)(ox) _{0.5}] _n	<i>P2</i> ₁ / <i>n</i>	<i>D</i> _{2d}	2	28	0.9×10 ⁻⁶	28
{[Dy(L ⁴)(H ₂ O)]·2CH ₃ CN} _n	<i>P</i> ̄ ₁	n.a.	1.5	53.5	3.0×10 ⁻⁷	29
{[Dy][Co(CN) ₆]}	<i>P</i> 6 ₃ /mmc	<i>D</i> _{3h}	0	51.8	1.76×10 ⁻⁶	30
{[Dy ₂ (L ⁵) ₃ (H ₂ O) ₄]·(acetone) ₂ ·(H ₂ O) ₃ } _n	<i>P</i> na2 ₁	<i>C</i> _{2v} , <i>D</i> _{2d}	0	1.9	9.7×10 ⁻⁵	31
[Dy(STP)(1,2-bdc)] _n	<i>P2</i> ₁ / <i>n</i>	<i>D</i> _{2d}	0	55.7	1.4×10 ⁻⁷	32
{[Dy ₆ (H ₂ O) ₂₄ [Co ₄ (tpatox) ₄]](NO ₃) ₆ ·53H ₂ O	<i>F</i> m̄3	<i>C</i> _{2v}	1	4.7	3.2×10 ⁻⁶	33
{[Dy ₂ L ³ ₂ (bpdo) ₂ (H ₂ O)(CH ₃ OH)]·2ClO ₄ ·2C H ₃ CN} _n	<i>P</i> n	<i>C</i> _{2v}	0	133	6.53×10 ⁻¹¹	34
{[Dy _{0.1} Y _{0.9} (dhbdc) _{1.5} (DMF) ₂]·DMF} _n	<i>P</i> ̄ ₁	<i>D</i> _{4d}	1	31.6	2×10 ⁻⁸	35
[Dy ₃ (pta) ₄ (Hpta)(H ₂ O)]·6H ₂ O	<i>P</i> 2 ₁ / <i>m</i>	<i>C</i> _s	0	126.0	9×10 ⁻¹⁰	36
[Dy(H ₂ pxdp) _{1.5}] _n	<i>P</i> ̄ ₁	<i>O</i> _h	0.5	51.2	3.9×10 ⁻⁷	37
Dy ₂ (amp ₂ H ₂) ₂ (C ₂ O ₄)(H ₂ O) ₂ ·10H ₂ O	<i>P</i> ̄ ₁	<i>D</i> _{2d}	0	41.5	2.2×10 ⁻⁵	This Work

H₂TDA = thiophen-2,5-dicarboxylic acid; H₂BPDC = 2,2'-bipyridine-5,5'-dicarboxylic acid; H₃BTC = 1,3,5-benzenetricarboxylic acid; ox = oxalate dianion; bipyNO = 4,4'-bipyridyl-N,N'-dioxide, TfO = triflate; H₃stp = 2-sulfoterephthalic acid; phen = 1,10-phenanthroline, H₃L¹ = 5-hydroxyisophthalic acid; EMIM = 1-ethyl-3-methylimidazolium, H₂BDC = 1,4-benzenedicarboxylic acid; H₃PIDC = 2-(pyridine-4-yl)-1H-imidazole-4,5-dicarboxylic acid; H₂FDA = furan-2,5-dicarboxylic acid, DMF = dimethylformamid; HINO = isonicotinic acid *N*-oxide; 1*H*-5-Cl-6-Opy-3-CO₂⁻ = 1-hydro-5-chloro-6-oxopyridine-3-carboxylate; hfac = hexafluoroacetylacetone; bpdo = 4,4'-bipyridine-N,N'-dioxide; ant = 9,10-anthracenedicarboxylic acid; (NH₂)₂-bdc = 2,5-diaminoterephthalic; CNip = 5-cyanoisophthalate; H₃BTB = 1,3,5-tris(4-carboxyphenyl)benzene; H₂DMTDC = 3,4-dimethylthieno[2,3-*b*]thiophene-2,5-dicarboxylic acid; H₃L² = biphenyl-3'nitro-3,4'5-tricarboxylic acid; H₃TATB = 4,4',4"-s-triazine-2,4,6-triy-tribenzoic acid; H₂O-PDA = 1,2-phenylenediacetic acid; H₄abtc = 3,3',5,5'-azobenzene-tetracarboxylic acid; H₂L³ = N'-(2-hydroxy-benzylidene)-picolinohydrazide; 2,3-H₂pzdc = pyrazine-2,3-dicarboxylic acid; H₂OBA = 4, 4'-oxybis(benzoate) acid, Hatz = 3-amino-1,2,4-triazole; 3,4'-oba = 3,4'-oxybis(benzoate); H₃L⁴ = tri(4-carboxyphenyl) phosphane oxide; H₂L⁵ = pamoic acid; NaSTP = sodium 2-(2,2':6',2"-terpyridin-4'-yl)benzenesulfonate, H₂(1,2-bdc) = benzene-1,2-dicarboxylic acid; tpatox⁶⁻ = N,N',N"-tris(4-phenyl)aminetris(oxamate); dhbdc = 2,5-dihydroxyterephthalic acid; H₂pta = 2-(4-pyridyl)-terephthalic acid; H₄pxdp = p-xylenediphosphonic acid; n.a. = not available.

I. Primary characterization

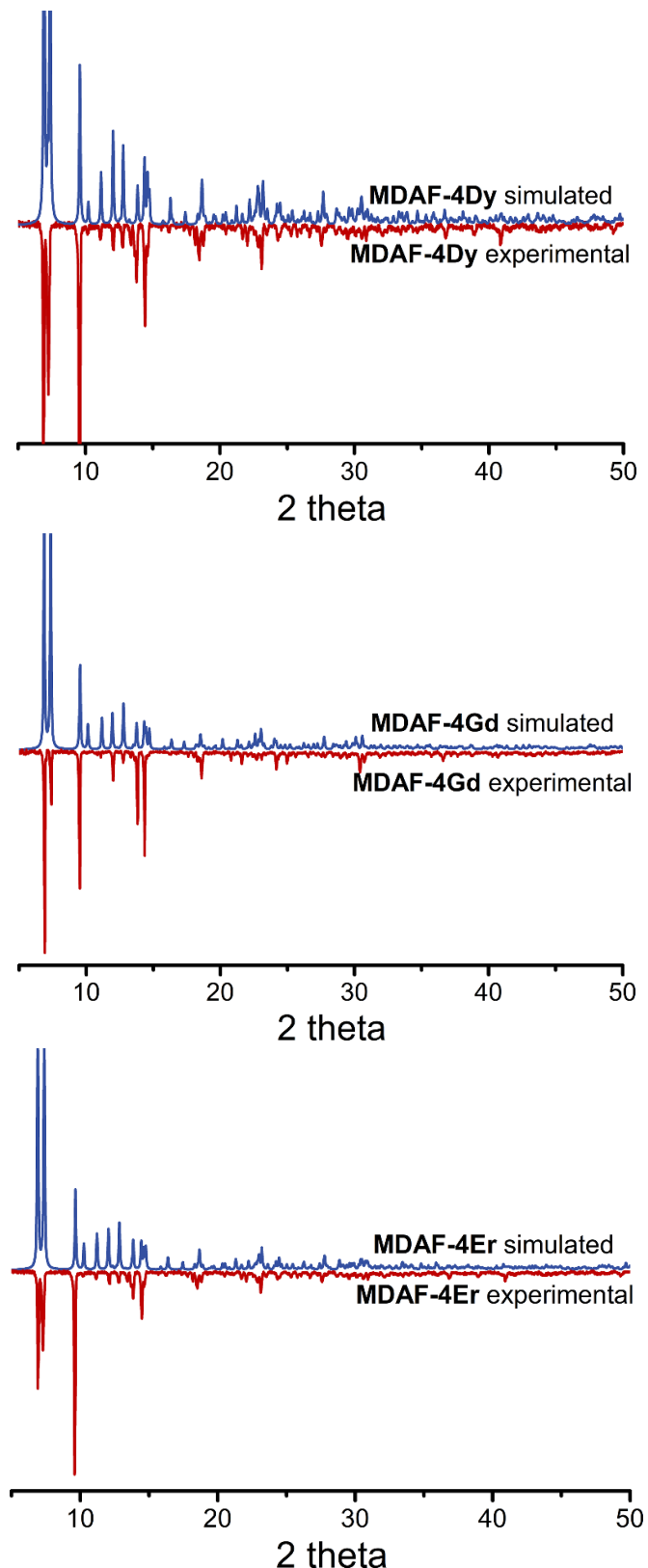


Figure S1. Experimental and simulated PXRD patterns of **MDAF-4Ln**.

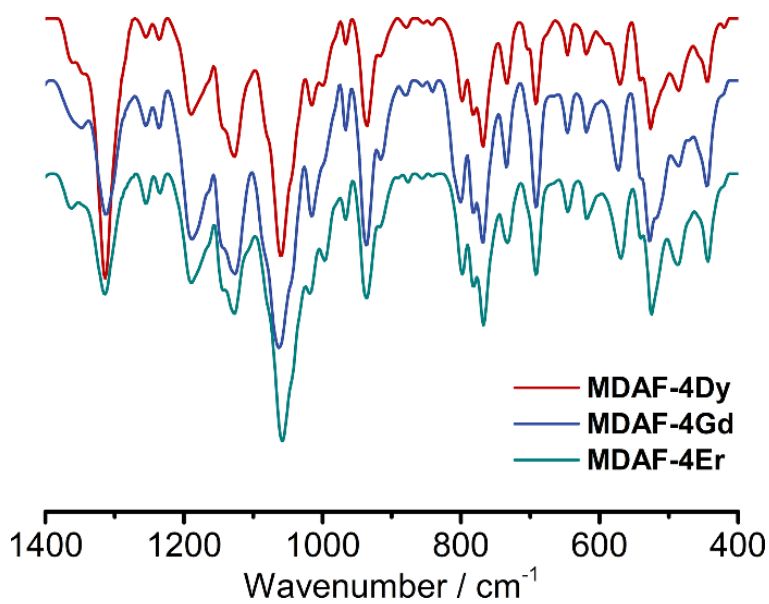
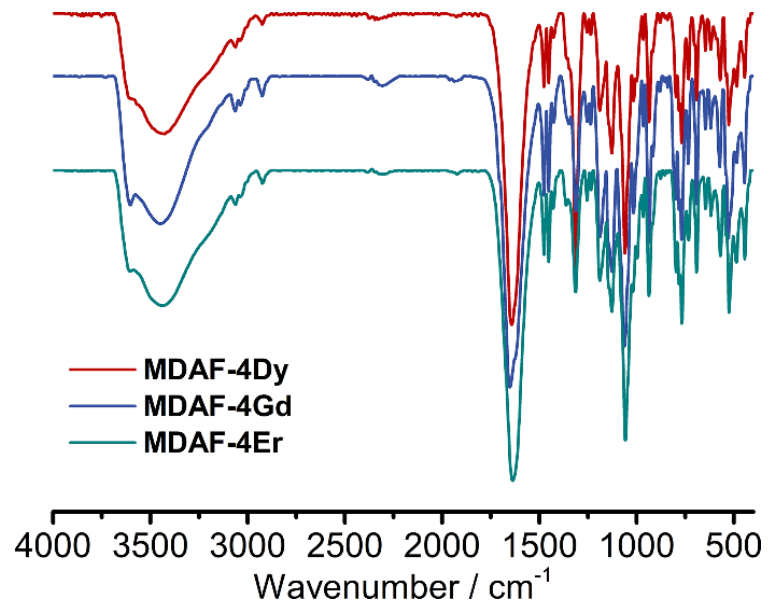


Figure S2. Infrared spectra of **MDAF-4Ln**.

II. Crystal structures

Table S2. Selected bond lengths (\AA) and bond angles ($^\circ$) for **MDAF-4Dy** at 193 K.

Dy1-O2	2.302(3)	O2-Dy1-O2A	74.07(10)
Dy1-O5	2.292(3)	O2-Dy1-O4A	77.30(10)
Dy1-O7	2.352(4)	O2-Dy1-O8B	134.24(10)
Dy1-O1A	2.361(3)	O5-Dy1-O7	103.58(13)
Dy1-O2A	2.568(3)	O1A-Dy1-O5	91.98(10)
Dy1-O4A	2.288(3)	O2A-Dy1-O5	74.24(10)
Dy1-O8B	2.404(3)	O4A-Dy1-O5	145.80(10)
Dy1-O1W	2.446(4)	O5-Dy1-O8B	137.82(9)
O1W-Dy1-O2	134.22(13)	O1A-Dy1-O7	147.73(12)
O1W-Dy1-O5	67.25(11)	O2A-Dy1-O7	152.38(11)
O1W-Dy1-O7	79.97(13)	O4A-Dy1-O7	95.85(12)
O1A-Dy1-O1W	80.35(12)	O7-Dy1-O8B	68.57(12)
O1W-Dy1-O2A	122.00(10)	O1A-Dy1-O2A	59.03(10)
O1W-Dy1-O4A	144.99(12)	O1A-Dy1-O4A	85.95(10)
O1W-Dy1-O8B	70.57(11)	O1A-Dy1-O8B	80.85(10)
O2-Dy1-O5	79.35(10)	O2A-Dy1-O4A	75.54(9)
O2-Dy1-O7	78.46(12)	O2A-Dy1-O8B	131.49(10)
O1A-Dy1-O2	132.82(10)	O4A-Dy1-O8B	75.54(10)

Symmetry codes: A: 1-x, -y, 1-z; B: 2-x, -y, 1-z.

Table S3. Coordination geometry for complexes **MDAF-4Ln**.

Coordination geometry	MDAF-4Dy	MDAF-4Gd	MDAF-4Er
Octagon (D_{8h})	31.997	31.877	31.843
Heptagonal pyramid (C_{7v})	22.700	22.495	22.889
Hexagonal bipyramid (D_{6h})	16.731	16.585	16.623
Cube (O_h)	10.962	10.990	11.219
Square antiprism (D_{4d})	3.322	3.428	3.320
Triangular dodecahedron (D_{2d})	0.944	0.979	0.927
Johnson gyrobifastigium J26 (D_{2d})	12.815	12.973	12.638
Johnson elongated triangular bipyramid J14 (D_{3h})	27.498	27.462	27.389
Biaugmented trigonal prism J50 (C_{2v})	2.758	2.738	2.714
Biaugmented trigonal prism (C_{2v})	2.415	2.322	2.381
Snub diphenoïd J84 (D_{2d})	2.616	2.722	2.558
Triakis tetrahedron (T_d)	11.373	11.453	11.665
Elongated trigonal bipyramid (D_{3h})	24.635	24.495	24.536

Table S4. Selected bond lengths (\AA) and bond angles ($^\circ$) for **MDAF-4Gd** at 193 K.

Gd1-O2	2.333(3)	O2-Gd1-O2A	73.83(10)
Gd1-O5	2.330(3)	O2-Gd1-O4A	76.79(10)
Gd1-O7	2.375(4)	O2-Gd1-O8B	134.27(12)
Gd1-O1A	2.387(4)	O5-Gd1-O7	104.65(14)
Gd1-O2A	2.578(3)	O1A-Gd1-O5	92.18(12)
Gd1-O4A	2.333(3)	O2A-Gd1-O5	73.91(10)
Gd1-O8B	2.431(3)	O4A-Gd1-O5	145.09(10)
Gd1-O1W	2.461(4)	O5-Gd1-O8B	138.07(12)
O1W-Gd1-O2	134.08(13)	O1A-Gd1-O7	147.68(12)
O1W-Gd1-O5	67.54(12)	O2A-Gd1-O7	152.41(11)
O1W-Gd1-O7	80.00(13)	O4A-Gd1-O7	95.12(12)
O1A-Gd1-O1W	81.37(12)	O7-Gd1-O8B	67.84(14)
O1W-Gd1-O2A	122.34(11)	O1A-Gd1-O2A	58.67(10)
O1W-Gd1-O4A	145.54(12)	O1A-Gd1-O4A	85.61(10)
O1W-Gd1-O8B	70.52(13)	O1A-Gd1-O8B	81.13(13)
O2-Gd1-O5	79.18(11)	O2A-Gd1-O4A	75.31(9)
O2-Gd1-O7	78.83(12)	O2A-Gd1-O8B	131.67(12)
O1A-Gd1-O2	132.15(10)	O4A-Gd1-O8B	76.03(12)

Symmetry codes: A: 1-x, -y, 1-z; B: 2-x, -y, 1-z.

Table S5. Selected bond lengths (\AA) and bond angles ($^\circ$) for **MDAF-4Er** at 193 K.

Er1-O2	2.275(4)	O2-Er1-O2A	72.69(14)
Er1-O5	2.287(4)	O2-Er1-O4A	77.39(15)
Er1-O7	2.320(4)	O2-Er1-O8B	135.15(14)
Er1-O1A	2.333(4)	O5-Er1-O7	103.24(15)
Er1-O2A	2.534(4)	O1A-Er1-O5	91.94(15)
Er1-O4A	2.272(4)	O2A-Er1-O5	74.36(14)
Er1-O8B	2.389(4)	O4A-Er1-O5	146.19(14)
Er1-O1W	2.418(4)	O5-Er1-O8B	137.42(14)
O1W-Er1-O2	134.63(15)	O1A-Er1-O7	147.86(14)
O1W-Er1-O5	67.25(15)	O2A-Er1-O7	151.64(14)
O1W-Er1-O7	79.98(14)	O4A-Er1-O7	95.81(14)
O1A-Er1-O1W	80.13(14)	O7-Er1-O8B	68.94(15)
O1W-Er1-O2A	122.47(14)	O1A-Er1-O2A	59.72(14)
O1W-Er1-O4A	144.66(15)	O1A-Er1-O4A	86.17(15)
O1W-Er1-O8B	70.17(14)	O1A-Er1-O8B	80.65(14)
O2-Er1-O5	79.13(14)	O2A-Er1-O4A	75.63(13)
O2-Er1-O7	79.08(15)	O2A-Er1-O8B	131.87(15)
O1A-Er1-O2	132.17(14)	O4A-Er1-O8B	75.56(14)

Symmetry codes: A: 1-x, -y, 1-z; B: 2-x, -y, 1-z.

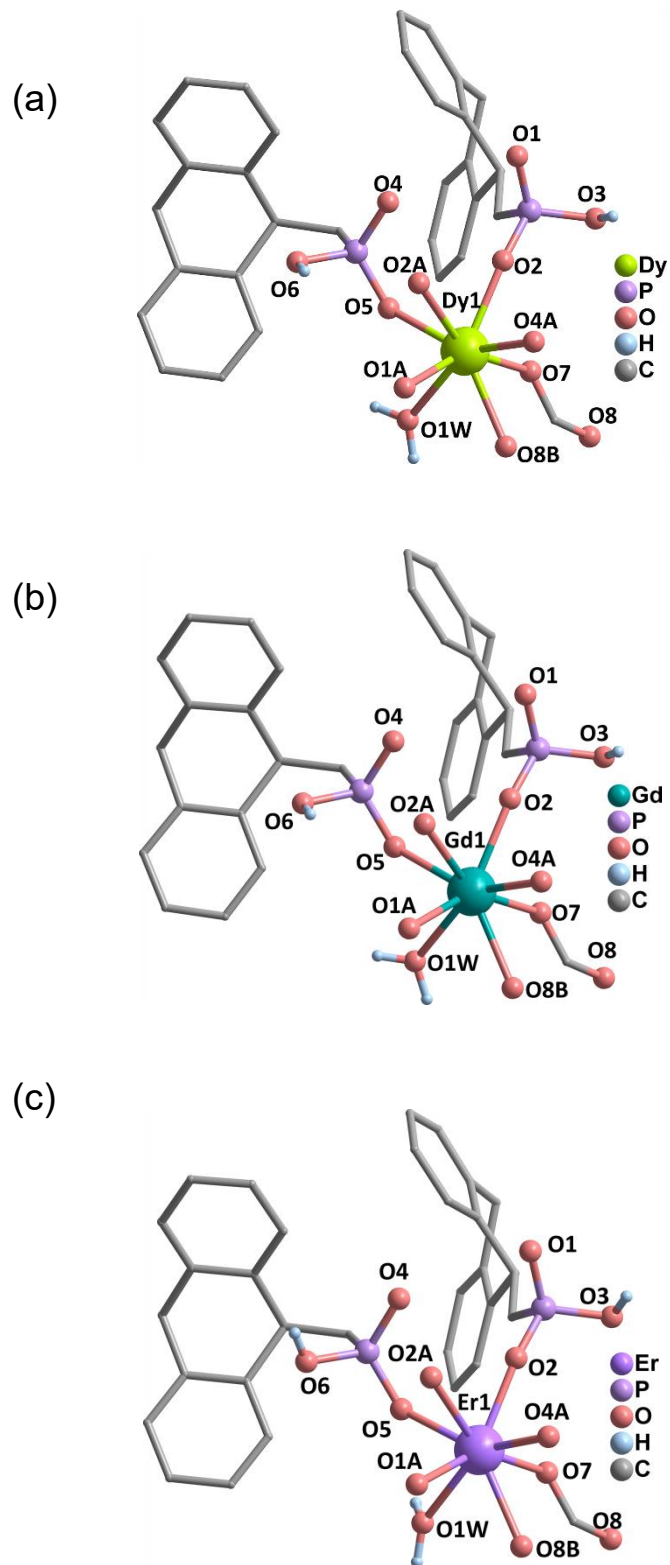


Figure S3. The asymmetric units of (a) **MDAF-4Dy**, (b) **MDAF-4Gd**, and (c) **MDAF-4Er**. All H atoms except those in coordination water and phosphonic groups are omitted for clarity.

III. Sorption properties

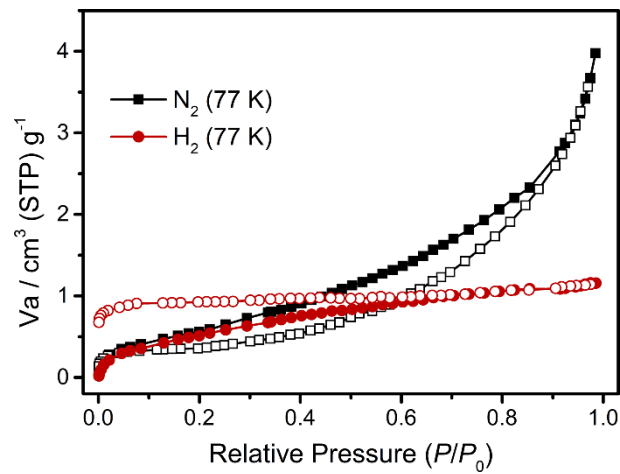


Figure S4. Adsorption (filled) and desorption (open) isotherms of N₂ (77 K) and H₂ (77 K) for **MDAF-4Dy**.

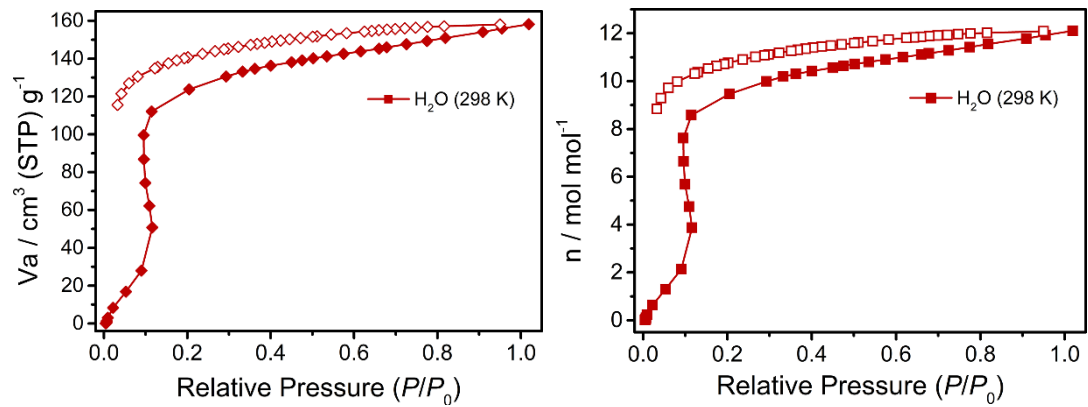


Figure S5. Adsorption (filled) and desorption (open) isotherms of H₂O (298 K) for **MDAF-4Dy**.

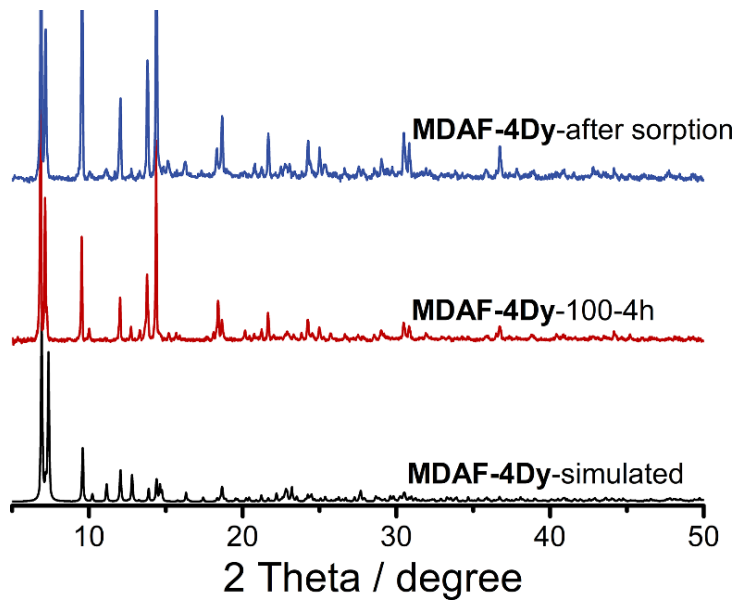


Figure S6. Powder X-ray diffraction patterns of **MDAF-4Dy**-simulated, **MDAF-4Dy**-100-4h (after thermal activation at 100°C under vacuum for 4 h) and **MDAF-4Dy**-after sorption.

IV. Thermo-induced phase transitions

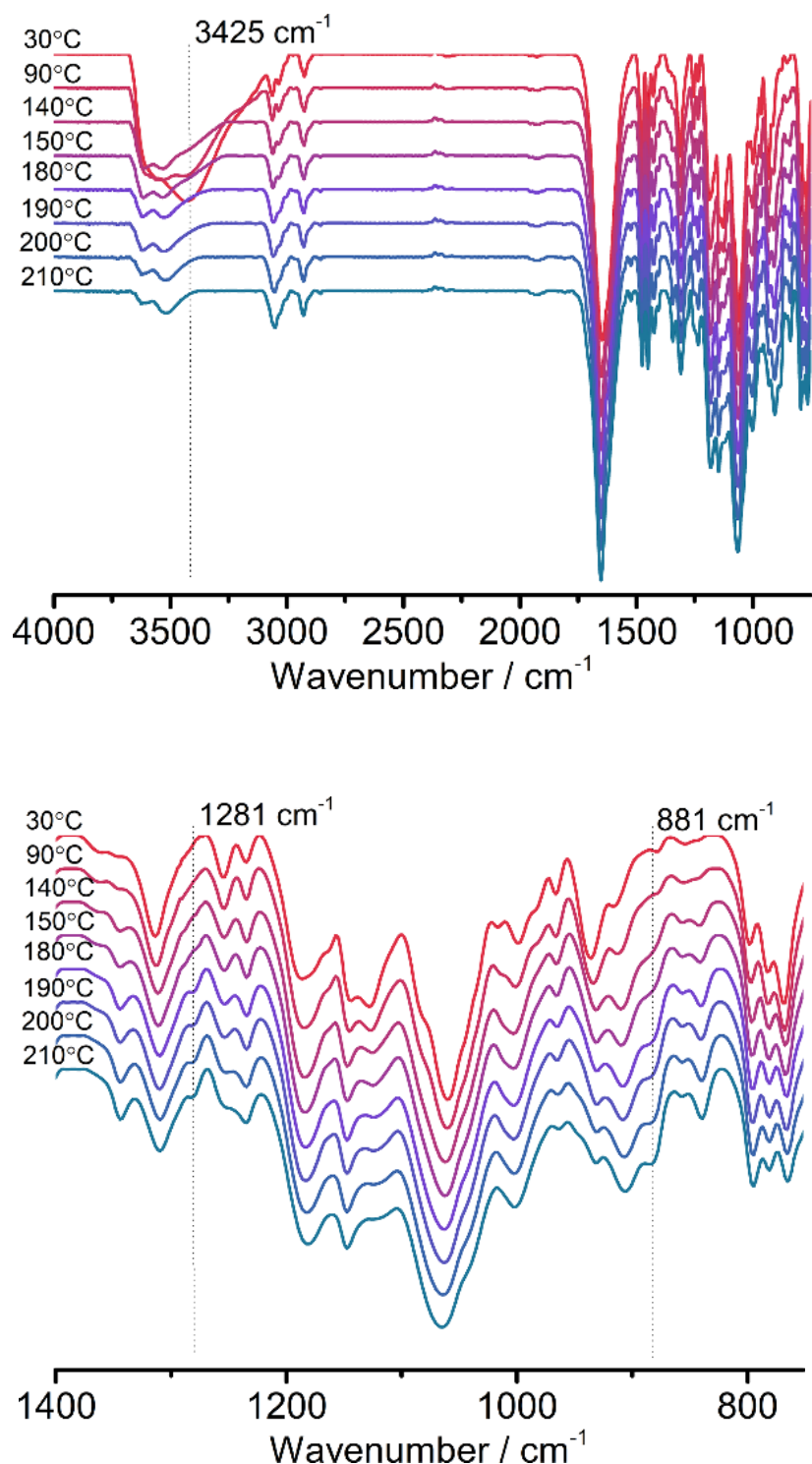


Figure S7. The in-situ variable temperature infrared (IR) spectra of **MDAF-4Dy** measured in the range of 30–210 °C.

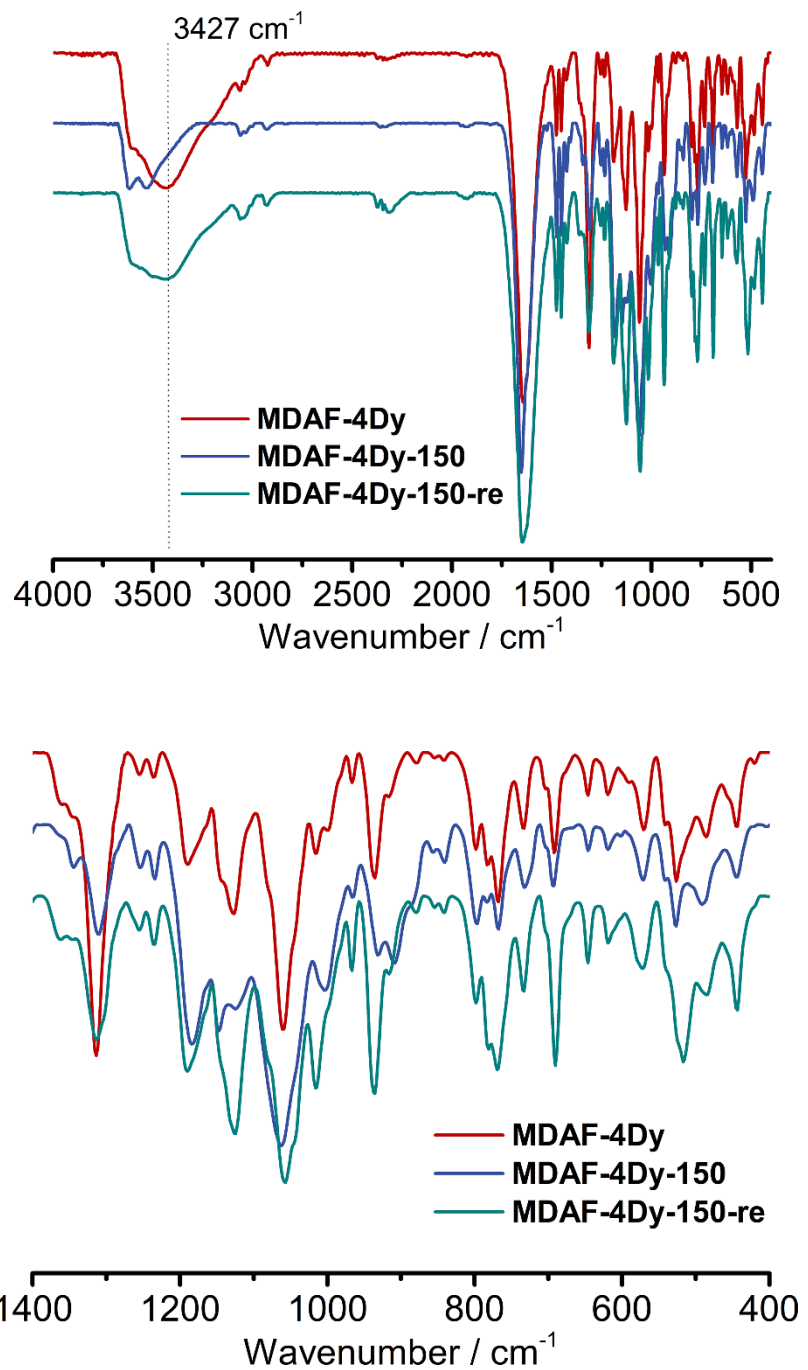


Figure S8. The IR spectra of **MDAF-4Dy**, the dehydration sample **MDAF-4Dy-150** and rehydration sample **MDAF-4Dy-150-re**.

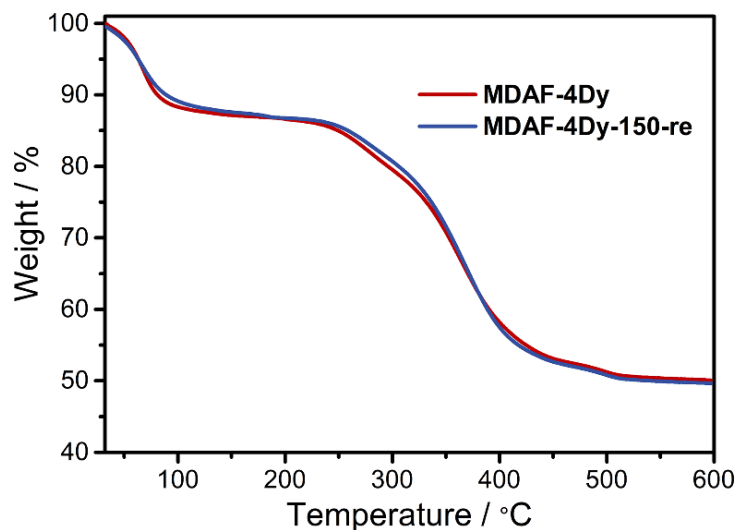


Figure S9. The TG plot of **MDAF-4Dy** and the rehydration sample **MDAF-4Dy-150-re**. **MDAF-4Dy-150-re** is obtained by immersing the dehydrated sample **MDAF-4Dy-150** in water for 1 day.

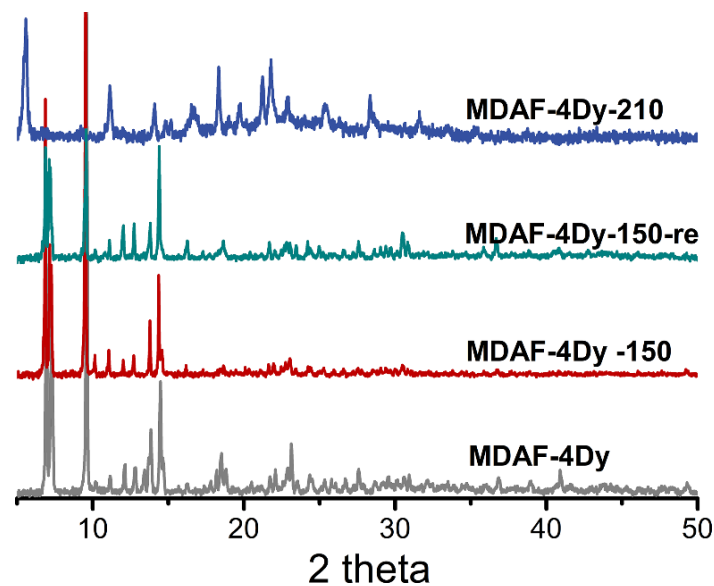


Figure S10. PXRD patterns of **MDAF-4Dy**, the dehydration sample **MDAF-4Dy-150**, rehydration sample **MDAF-4Dy-150-re** and the dedimerization sample **MDAF-4Dy-210**.

V. Optical properties

Table S6. The emission lifetimes at room temperature for **MDAF-4Dy**, **MDAF-4Dy-150**, **MDAF-4Dy-210** and **MDAF-4Gd**, **MDAF-4Er**, excited at 374 nm.

complex	$\lambda_{\text{em}} / \text{nm}$	τ_1 / ns	τ_2 / ns	$\tau_{\text{average}} / \text{ns}$	χ^2
MDAF-4Dy	430	1.72 (72 %)	7.58 (28 %)	3.35	1.07
	450	2.10 (73 %)	9.30 (27 %)	4.05	1.16
	485	2.26 (79 %)	12.16 (21 %)	4.33	1.09
MDAF-4Dy-150	432	1.52 (80 %)	4.10 (20 %)	2.04	1.15
	458	1.42 (82 %)	4.41 (18 %)	1.96	1.06
	485	1.86 (86 %)	7.89 (14 %)	2.69	1.03
MDAF-4Dy-210	470	1.26 (74 %)	3.51 (26 %)	1.84	1.18
MDAF-4Gd	429	2.51 (41 %)	7.53 (59 %)	5.49	1.05
	451	2.17 (43 %)	7.63 (57 %)	5.31	1.13
	478	2.25 (48 %)	8.34 (52%)	5.43	1.04
MDAF-4Er	430	1.42 (55 %)	8.11 (45 %)	4.42	1.08
	450	3.63 (65 %)	11.14 (35 %)	6.33	1.03
	480	1.06 (48 %)	7.21 (52%)	4.52	1.14

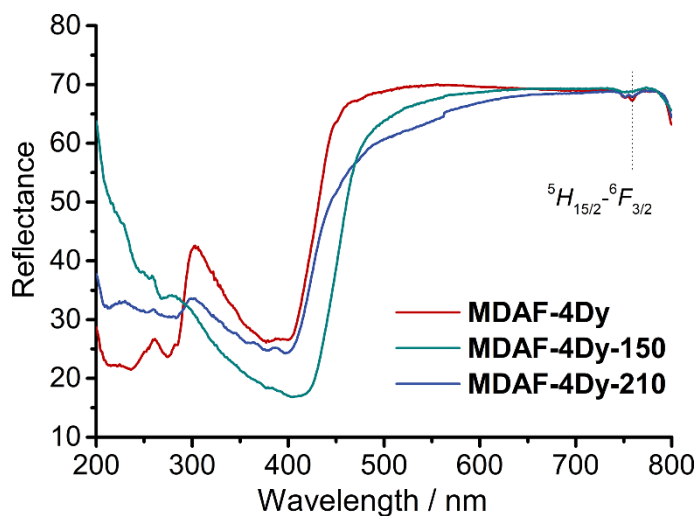


Figure S11. The UV-vis reflectance spectra for complexes **MDAF-4Dy**, **MDAF-4Dy-150** and **MDAF-4Dy-210**.

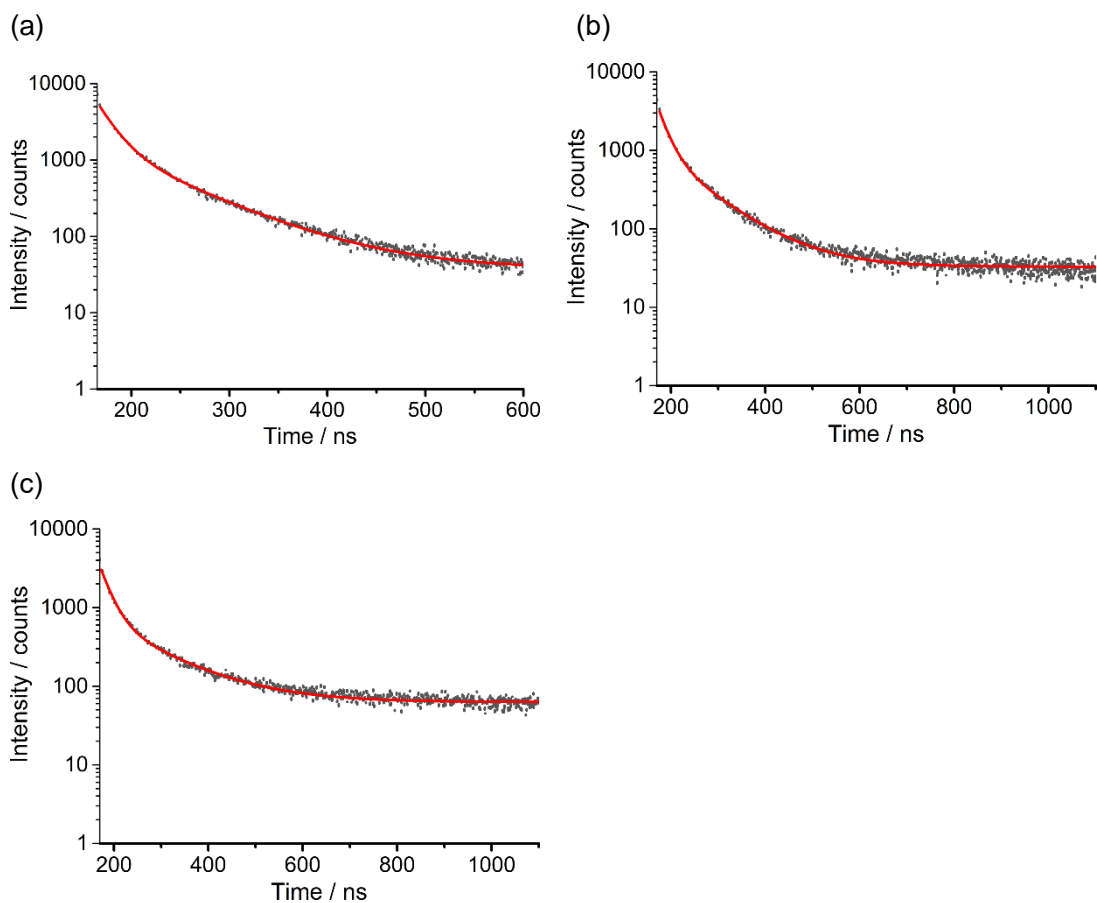


Figure S12. Fluorescence decay curve, fitting line and fitting residue for **MDAF-4Dy** emitting at (a) 430 nm, (b) 450 nm, and (c) 485 nm (excited at 374 nm). The decay profiles were fitted reasonably well to the double exponential equation via the software DAS6 attached to FluoroLog-UltraFast (HORIBA Instrument Inc, Edison).

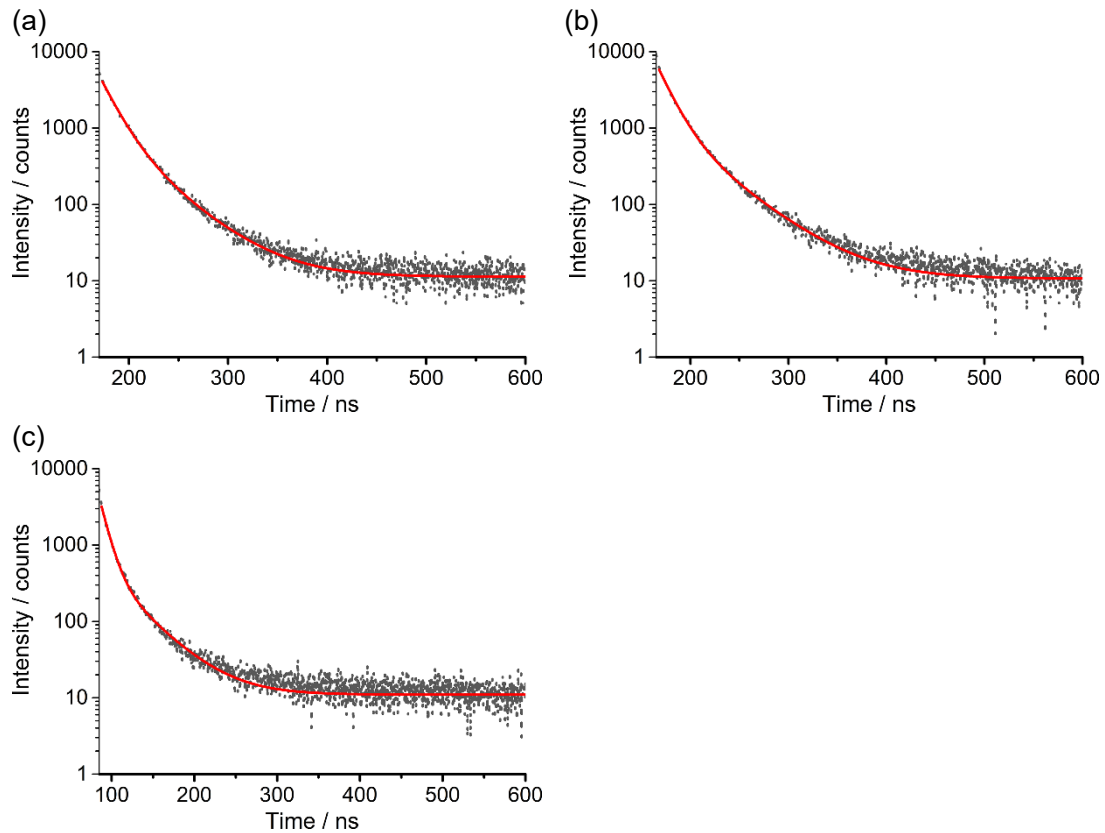


Figure S13. Fluorescence decay curve, fitting line and fitting residue for **MDAF-4Dy-150** emitting at (a) 432 nm, (b) 458 nm, and (c) 485 nm (excited at 374 nm). The decay profiles were fitted reasonably well to the double exponential equation via the software DAS6 attached to FluoroLog-UltraFast (HORIBA Instrument Inc, Edison).

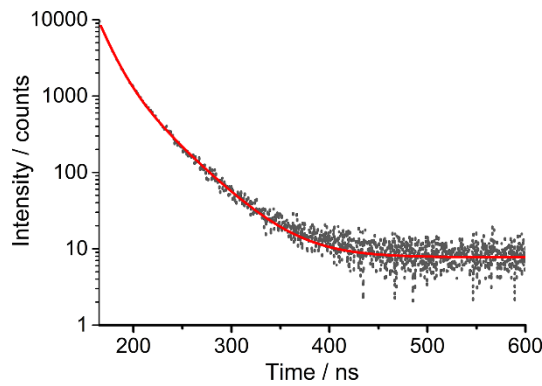


Figure S14. Fluorescence decay curve, fitting line and fitting residue for **MDAF-4Dy-210** emitting at 470 nm (excited at 374 nm). The decay profiles were fitted reasonably well to the double exponential equation via the software DAS6 attached to FluoroLog-UltraFast (HORIBA Instrument Inc, Edison).

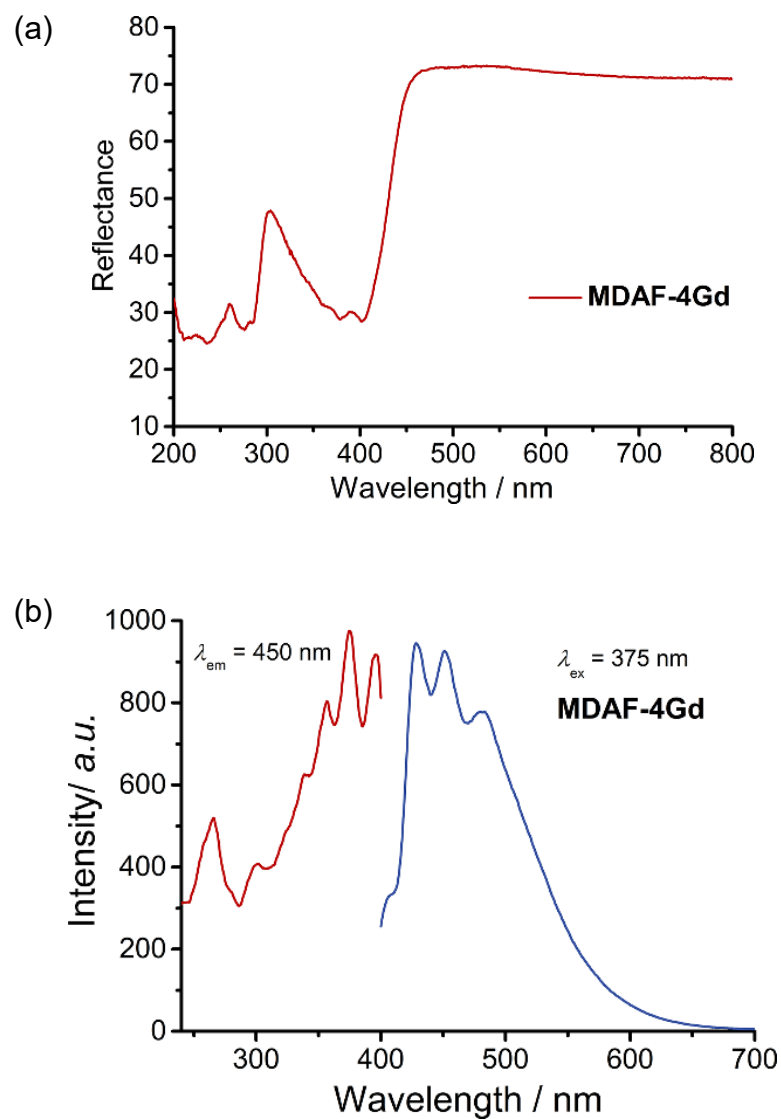


Figure S15. (a) The UV-vis reflectance spectra and (b) the steady state emission spectra excited at 375 nm for **MDAF-4Gd**.

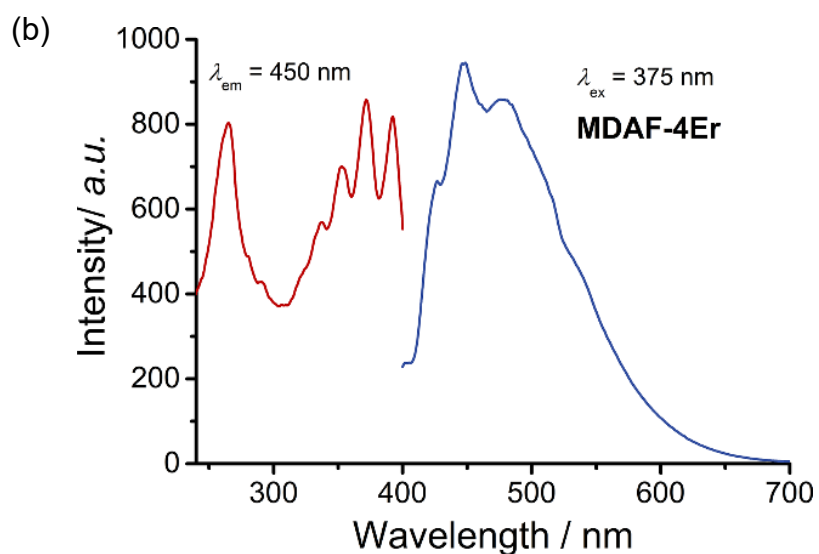
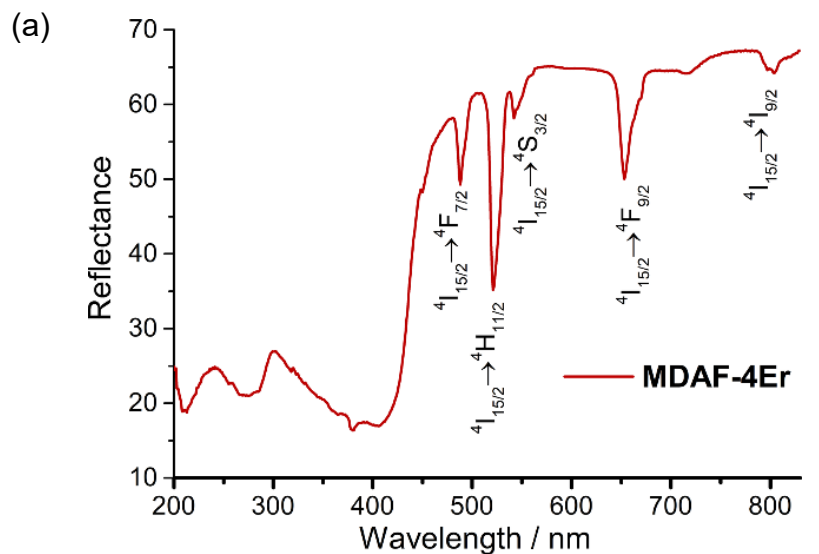


Figure S16. (a) The UV-vis reflectance spectra and (b) the steady state emission spectra excited at 375 nm for **MDAF-4Er**.

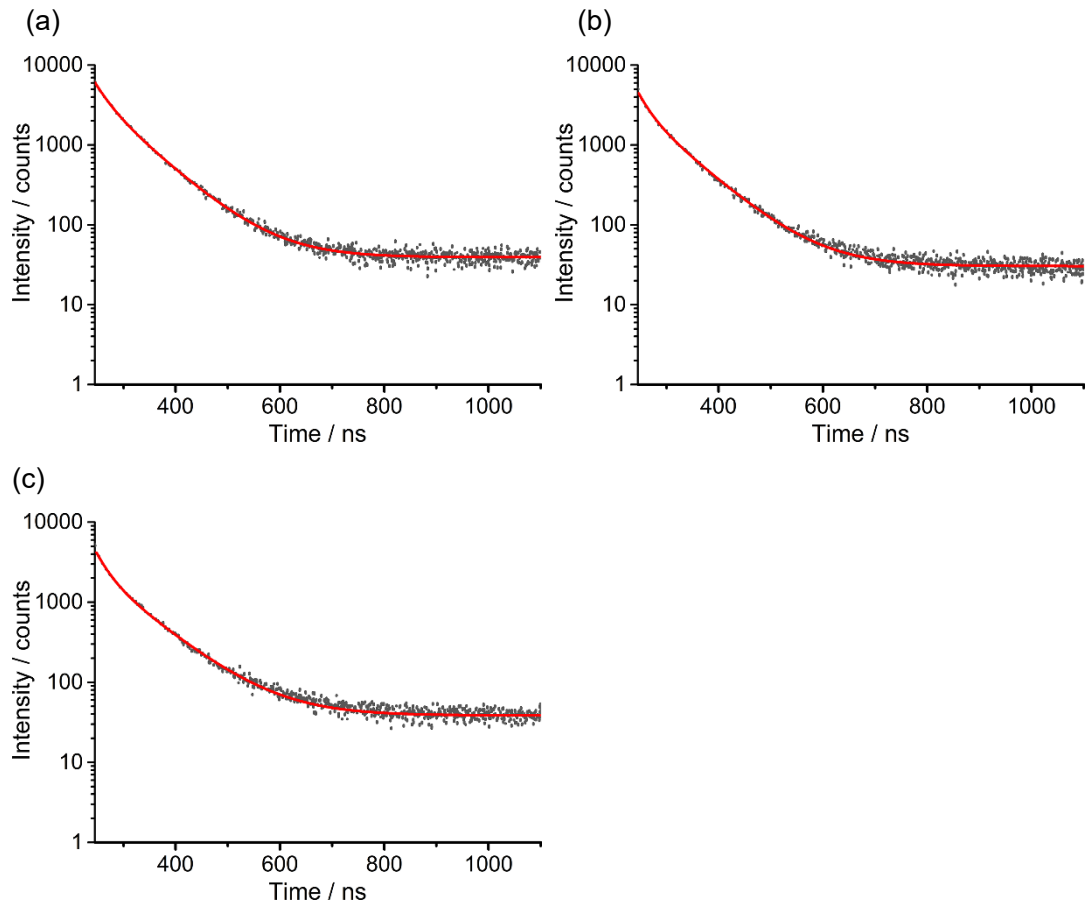


Figure S17. Fluorescence decay curve, fitting line and fitting residue for **MDAF-4Gd** emitting at (a) 429 nm, (b) 451 nm, and (c) 478 nm (excited at 374 nm). The decay profiles were fitted reasonably well to the double exponential equation via the software DAS6 attached to FluoroLog-UltraFast (HORIBA Instrument Inc, Edison).

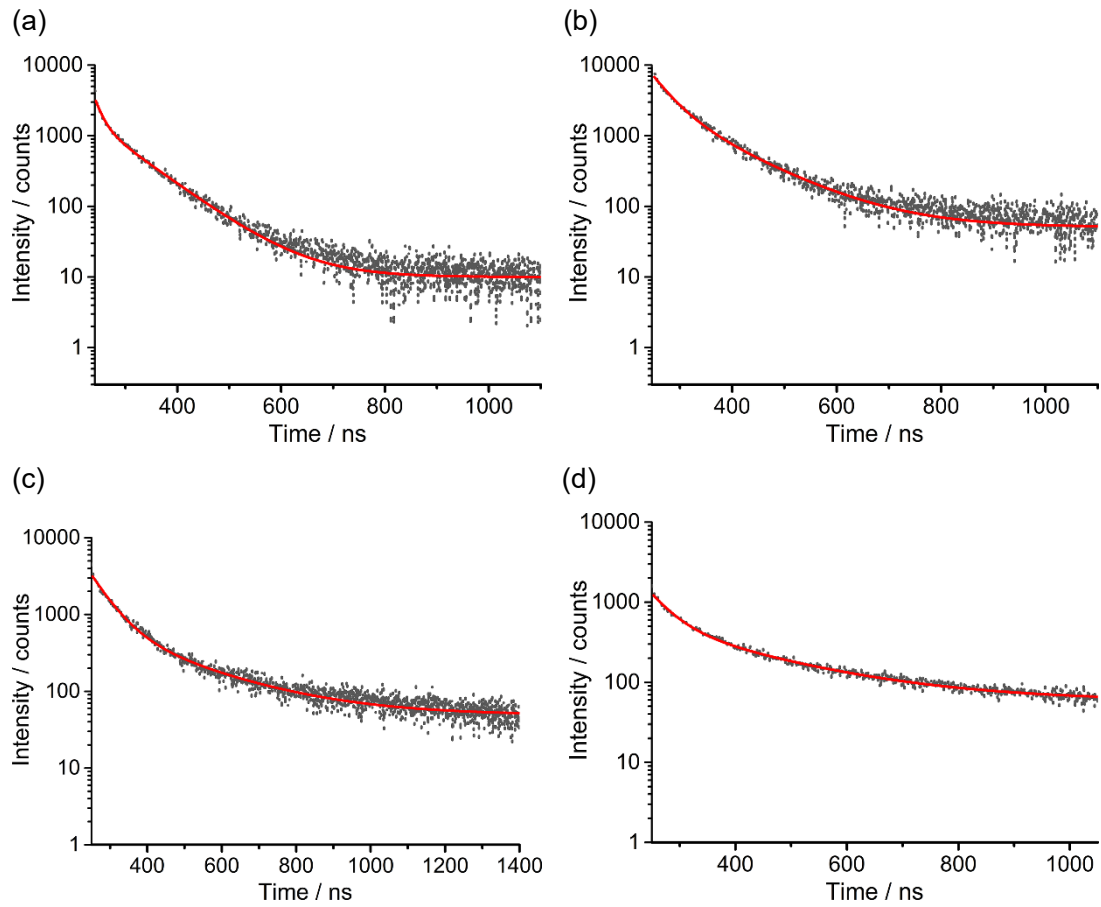


Figure S18. Fluorescence decay curve, fitting line and fitting residue for **MDAF-4Er** emitting at (a) 430 nm, (b) 450 nm, (c) 480 nm and (c) 530 nm (excited at 374 nm). The decay profiles were fitted reasonably well to the double exponential equation via the software DAS6 attached to FluoroLog-UltraFast (HORIBA Instrument Inc, Edison).

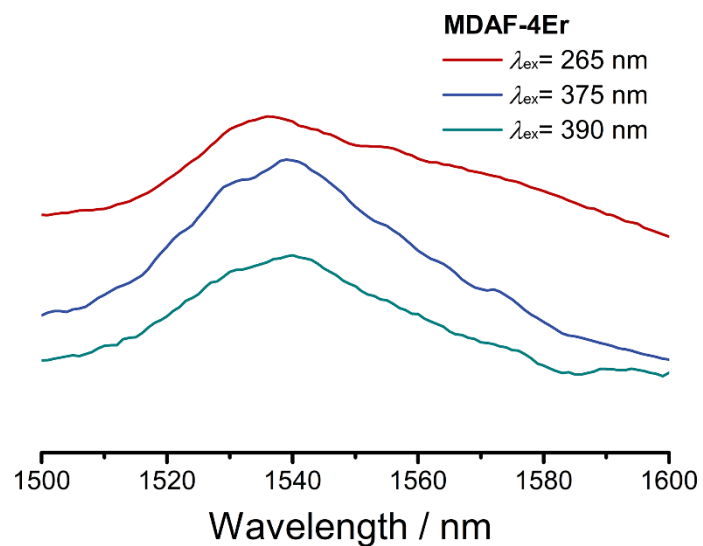


Figure S19. The near-infrared emission spectra for the solid complexes **MDAF-4Er** at different excited wavelengths.

VI. Magnetic studies

Table S7. The fit parameters obtained from analyses of the ac susceptibilities of **MDAF-4Dy** under zero dc field.

T / K	$\chi\tau^l$ / cm ³ mol ⁻¹	χs^l / cm ³ mol ⁻¹	ln(τ / s)	α	Residual
2	10.94	5.24	-2.67	0.55	1.30 E-1
2.5	9.13	4.21	-2.69	0.51	7.09 E-2
3	7.89	3.53	-2.77	0.49	4.82 E-2
3.5	6.97	3.07	-2.87	0.48	3.21 E-2
4	6.23	2.73	-3.01	0.47	2.32 E-2
5	5.11	2.29	-3.48	0.44	1.79 E-2
6	4.30	2.02	-4.15	0.40	1.29 E-2
7	3.73	1.83	-4.82	0.36	1.05 E-2
8	3.30	1.70	-5.43	0.33	1.22 E-2
9	2.96	1.63	-5.98	0.30	1.02 E-2
10	2.69	1.56	-6.48	0.28	8.38 E-3
11	2.46	1.51	-7.00	0.27	8.26 E-3
12	2.28	1.49	-7.50	0.28	8.67 E-3

Table S8. The fit parameters obtained from analyses of the ac susceptibilities of **MDAF-4Dy-150** under zero dc field.

T / K	$\chi\tau^l$ / cm ³ mol ⁻¹	χs^l / cm ³ mol ⁻¹	ln(τ / s)	α	Residual
2	7.99	2.88	-4.75	0.67	5.04 E-2
2.5	6.89	2.57	-4.76	0.65	3.43 E-2
3	6.02	2.36	-4.73	0.63	2.82 E-2
3.5	5.34	2.15	-4.76	0.61	1.99 E-2
4	4.76	2.01	-4.92	0.58	1.71 E-2
5	3.95	1.79	-5.32	0.54	1.37 E-2
6	3.37	1.62	-5.88	0.51	1.10 E-2
7	2.95	1.51	-6.44	0.50	9.45 E-3
8	2.61	1.52	-6.72	0.46	1.38 E-2
9	2.34	1.53	-6.93	0.41	1.01 E-2
10	2.12	1.51	-7.20	0.38	9.28 E-3
11	1.95	1.48	-7.42	0.35	7.30 E-3
12	1.79	1.48	-7.48	0.30	7.59 E-3

Table S9. The fit parameters obtained from analyses of the ac susceptibilities of **MDAF-4Dy-150-re** under zero dc field.

T / K	χ_{irr} / cm ³ mol ⁻¹	χ_{sus} / cm ³ mol ⁻¹	ln(τ / s)	α	Residual
2	9.14	3.54	-2.91	0.63	1.27 E-1
2.5	7.64	2.96	-2.93	0.59	9.01 E-2
3	6.67	2.55	-2.96	0.56	8.35 E-2
3.5	5.92	2.24	-3.01	0.56	7.06 E-2
4	5.33	2.03	-3.20	0.54	3.87 E-2
5	4.28	1.72	-3.82	0.50	3.91 E-2
6	3.52	1.56	-4.51	0.45	3.37 E-2
7	3.16	1.43	-5.03	0.42	2.94 E-2
8	2.71	1.34	-5.75	0.39	1.69 E-2
9	2.42	1.31	-6.31	0.33	2.10 E-2
10	2.18	1.29	-6.76	0.30	1.97 E-2
11	2.02	1.24	-7.25	0.31	2.03 E-2
12	1.86	1.24	-7.69	0.29	1.92 E-2

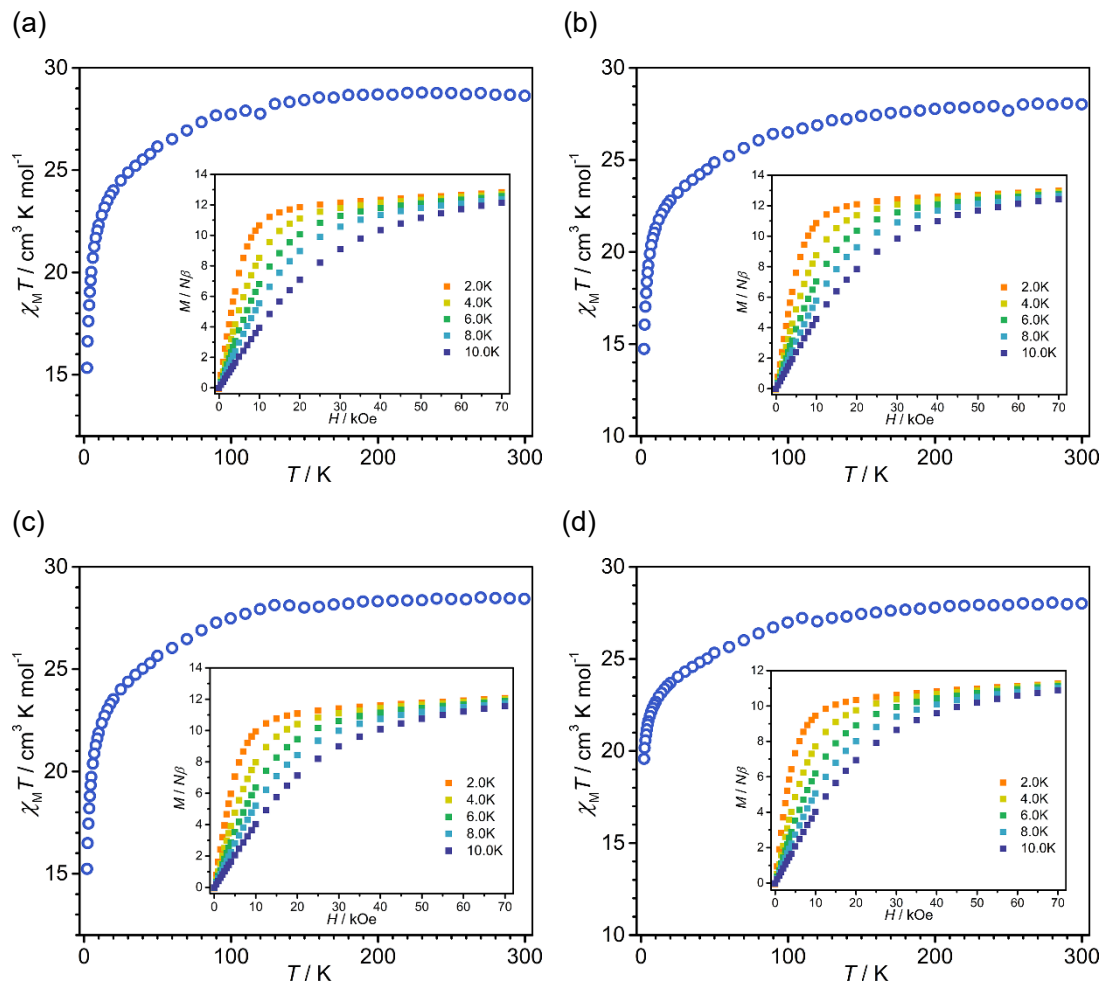


Figure S20. Temperature dependence of $\chi_M T$ on cooling in a field of 1 kOe for (a) **MDAF-4Dy**, (b) **MDAF-4Dy-150**, (c) **MDAF-4Dy-150-re** and (d) **MDAF-4Dy-210**. Inset: Field dependence of the magnetization at depicted temperature.

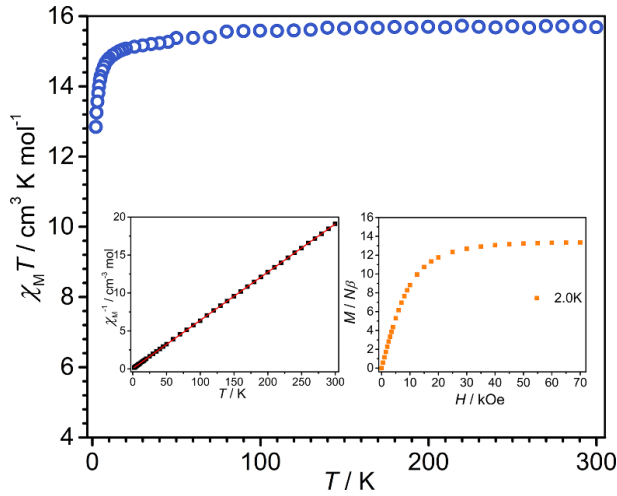


Figure S21. Temperature dependence of $\chi_M T$ on cooling in a field of 1 kOe for the Gd analogues **MDAF-4Gd**. Inset: The χ_M^{-1} vs. T curve and the field dependence of the magnetization at 2 K.

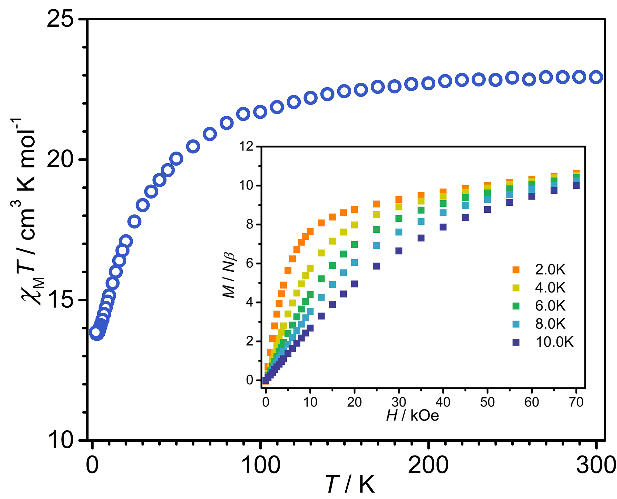


Figure S22. Temperature dependence of $\chi_M T$ on cooling in a field of 1 kOe for the Er analogues **MDAF-4Er**. Inset: Field dependence of the magnetization at depicted temperature.

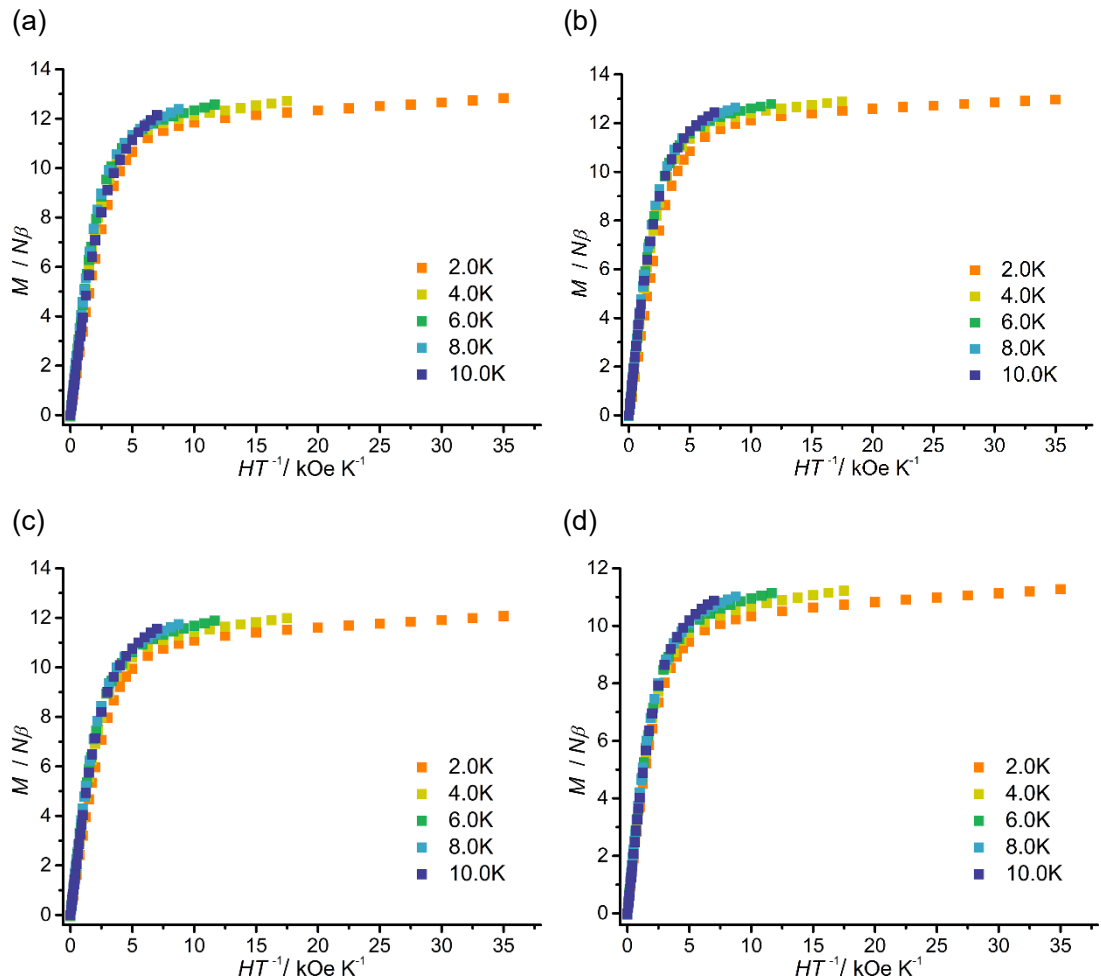


Figure S23. The plots of magnetization M versus H/T at depicted temperatures for complexes (a) MDAF-4Dy, (b) MDAF-4Dy-150, (c) MDAF-4Dy-150-re and (d) MDAF-4Dy-210.

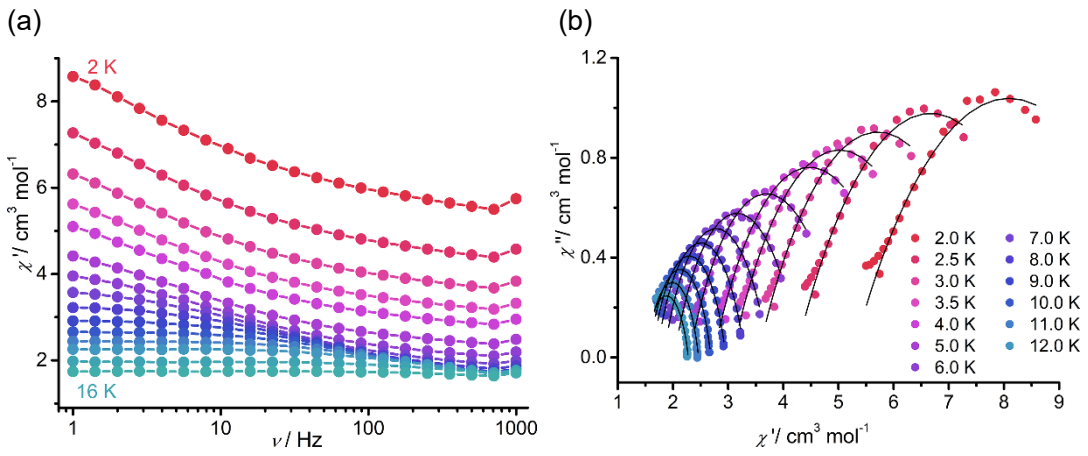


Figure S24. (a) Frequency dependence of the in-phase (χ') ac susceptibilities for **MDAF-4Dy** measured in the temperatures range 2-16 K under zero dc field. (b) Cole-Cole plots for **MDAF-4Dy** measured in the temperatures range 2-12 K under zero dc field. The solid line represents the best fit using a generalized Debye model.

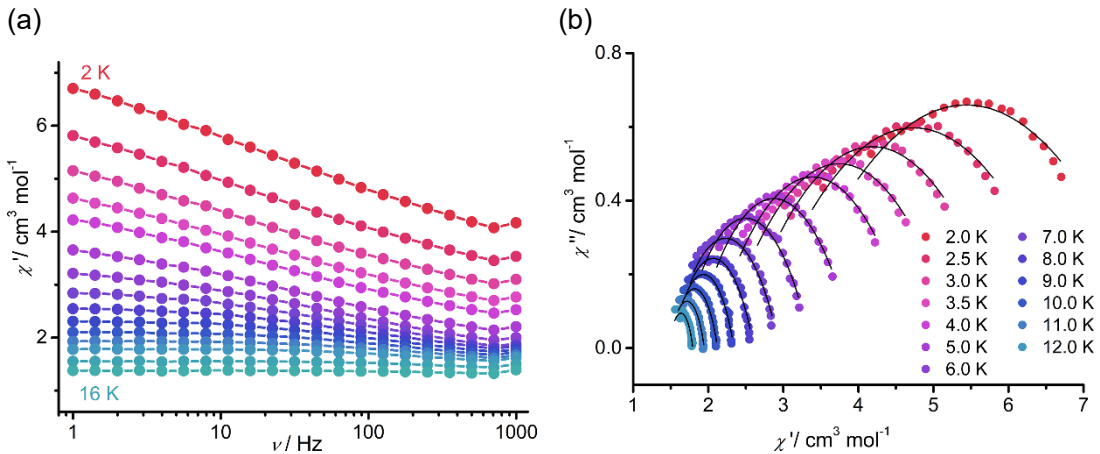


Figure S25. (a) Frequency dependence of the in-phase (χ') ac susceptibilities for **MDAF-4Dy-150** measured in the temperatures range 2-16 K under zero dc field. (b) Cole-Cole plots for **MDAF-4Dy-150** measured in the temperatures range of 2-12 K under zero dc field. The solid line represents the best fit using a generalized Debye model.

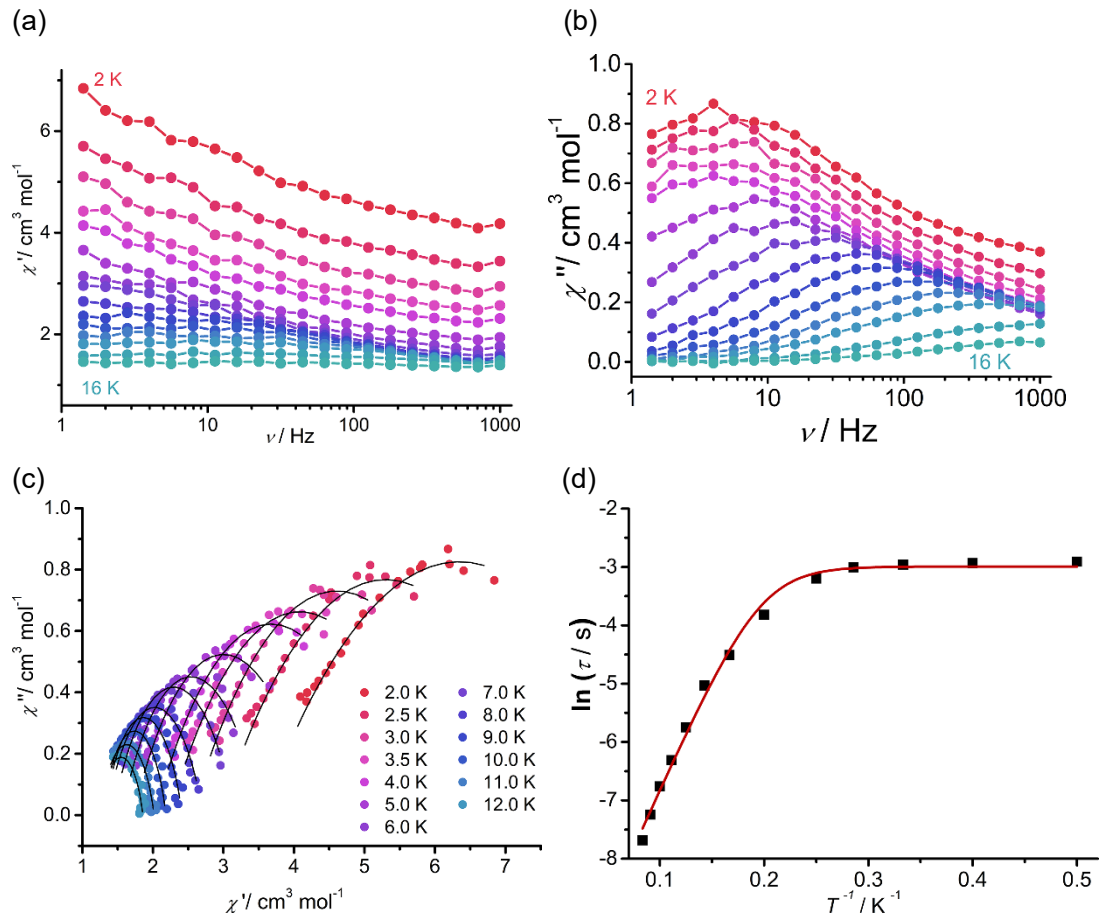


Figure S26. Frequency dependence of χ' (a) and χ'' (b) signals for **MDAF-4Dy-150-re** measured in the temperatures range 2-16 K under zero dc field. (c) Cole-Cole plots for **MDAF-4Dy-150-re** measured in the temperatures range of 2-12 K under zero dc field. The solid line represents the best fit using a generalized Debye model. (d) Plots of $\ln \tau$ vs. T^{-1} for **MDAF-4Dy-150-re**.

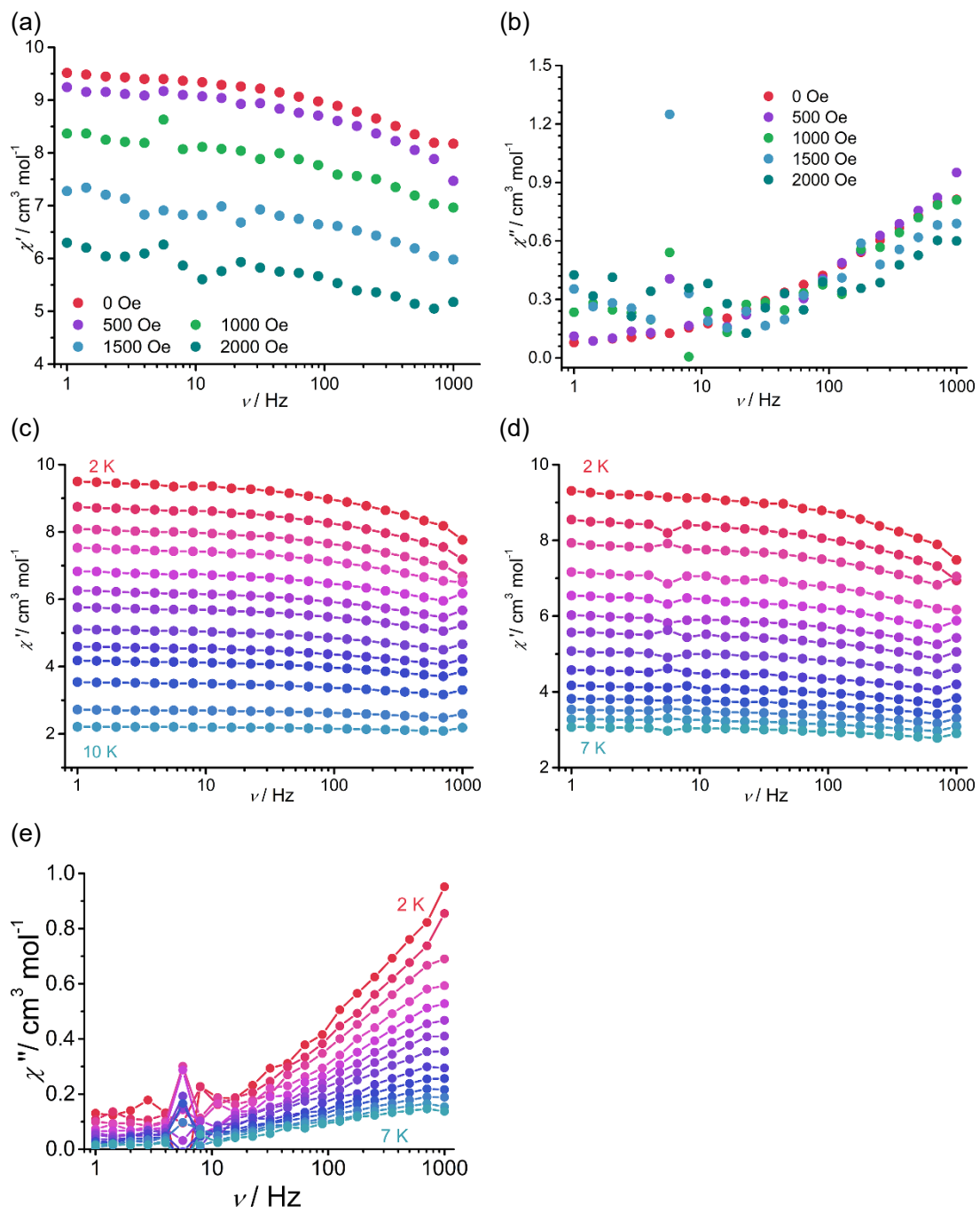


Figure S27. Frequency dependence of χ' (a) and χ'' (b) signals for **MDAF-4Dy-210** in the indicated dc fields at 2 K. (c) Frequency dependence of χ' for **MDAF-4Dy-210** measured in the temperatures range 2-10 K under zero dc field. Frequency dependence of χ' (d) and χ'' (e) for **MDAF-4Dy-210**, measured in the temperature range 2-7 K under 500 Oe dc field.

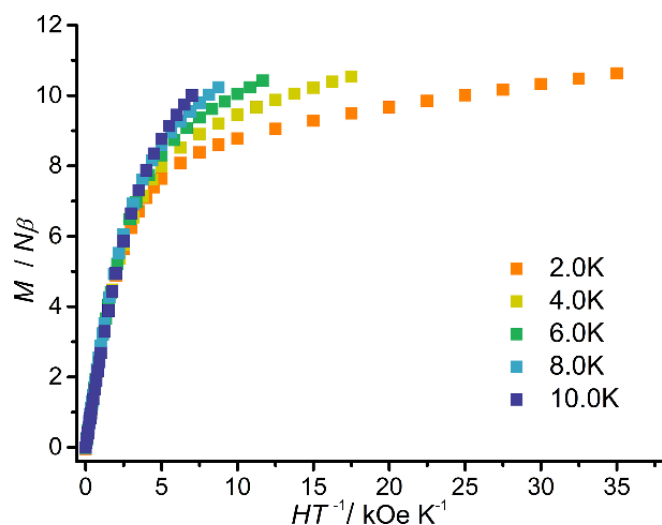


Figure S28. The plots of magnetization M versus H/T at depicted temperatures for complex **MDAF-4Er**.

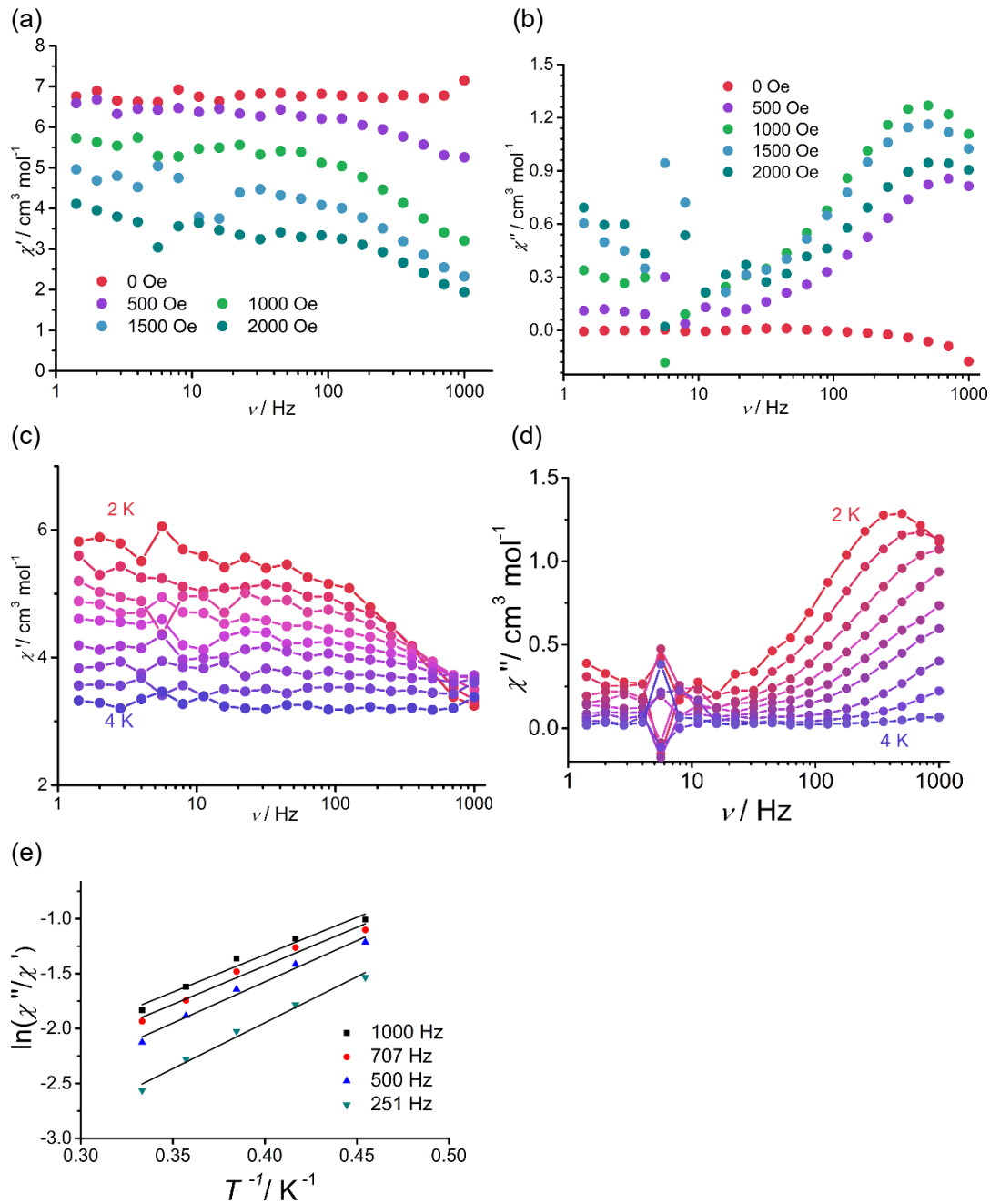


Figure S29. Frequency dependence of χ' (a) and χ'' (b) signals for **MDAF-4Er** in the indicated dc fields at 2 K. Frequency dependence of χ' (c) and χ'' (d) for **MDAF-4Er**, measured in the temperature range 2 - 4 K under 1000 Oe dc field. (e) Plots of $\ln(\chi''/\chi')$ versus T^{-1} for **MDAF-4Er** under 1000 Oe dc field.

VII. Magnetic computational details

Complex **MDAF-4Dy** is a three-dimensional MOF containing Dy-chain which has only one type of Dy^{III} fragment. Complete-active-space self-consistent field (CASSCF) calculations on one type of individual Dy^{III} fragment (see Figure S30 for the calculated model structures) on the basis of single-crystal X-ray determined geometries have been carried out with MOLCAS 8.4³⁸ program package. The huge demand of computational resources severely limits its applicability to large molecules, and thus we simplified the fragments and replaced the neighboring Dy^{III} ions by diamagnetic Lu^{III}. The influence of the next nearest neighboring Dy^{III} ions was taken into account by the closed-shell La^{III} ab initio embedding model potentials (AIMP; La.ECP.deGraaf.0s.0s.0e-La-(LaMnO₃).³⁹

The basis sets for all atoms are atomic natural orbitals from the MOLCAS ANO-RCC library: ANO-RCC-VTZP for Dy^{III}; VTZ for close O; VDZ for distant atoms. The calculations employed the second order Douglas-Kroll-Hess Hamiltonian, where scalar relativistic contractions were taken into account in the basis set and the spin-orbit couplings were handled separately in the restricted active space state interaction (RASSI-SO) procedure. For individual Dy^{III} fragment, active electrons in 7 active orbitals include all f electrons (CAS (9 in 7)) in the CASSCF calculation. To exclude all the doubts, we calculated all the roots in the active space. We have mixed the maximum number of spin-free state which was possible with our hardware (all from 21 sextets, 128 from 224 quadruplets, 130 from 490 doublets). SINGLE_ANISO⁴⁰ program was used to obtain the energy levels, g tensors, predominant m_J values, magnetic axes, *et al.* based on the above CASSCF/RASSI-SO calculations.

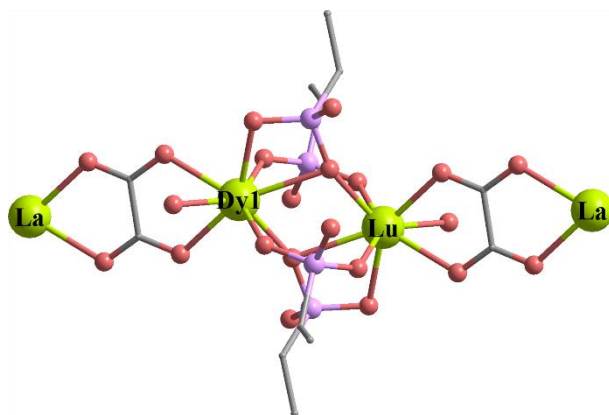


Figure S30. Calculated structure of individual Dy^{III} fragment in **MDAF-4Dy**.

Table S10. Calculated energy levels (cm^{-1}), g (g_x , g_y , g_z) tensors and predominant m_J values of the lowest eight Kramers doublets (KDs) of individual Dy^{III} fragment in **MDAF-4Dy** using CASSCF/RASSI-SO with MOLCAS 8.4.

KDs	MDAF-4Dy		
	E/cm^{-1}	g_x, g_y, g_z	m_J
1	0.0	0.023, 0.038, 19.501	$\pm 15/2$
2	122.0	2.135, 5.767, 13.820	$\pm 7/2$
3	150.9	2.700, 5.050, 8.584	$\pm 11/2$
4	222.4	3.756, 5.772, 9.380	$\pm 5/2$
5	270.8	0.646, 3.778, 12.235	$\pm 9/2$
6	291.1	1.853, 4.182, 12.215	$\pm 1/2$
7	349.6	0.094, 0.138, 16.381	$\pm 13/2$
8	423.4	0.009, 0.023, 19.382	$\pm 3/2$

Table S11. Wave functions with definite projection of the total moments $|m_J\rangle$ for the lowest two KDs of individual Dy^{III} fragment in **MDAF-4Dy** using CASSCF/RASSI-SO with MOLCAS 8.4.

	E/cm^{-1}	wave functions
MDAF-4Dy	0.0	93.71% $ \pm 15/2\rangle$ +5.23% $ \pm 11/2\rangle$
	122.0	25.26% $ \pm 13/2\rangle$ +25.95% $ \pm 1/2\rangle$ +20.39% $ \pm 3/2\rangle$ +15.83% $ \pm 5/2\rangle$

To fit the exchange interactions in **MDAF-4Dy**, we took two steps to obtain them. Firstly, we calculated individual Dy^{III} fragment using CASSCF/RASSI-SO to obtain the corresponding magnetic properties. Then, the exchange interaction between the magnetic centers is considered within the Lines model,⁴¹ while the account of the dipole-dipole magnetic coupling is treated exactly. The Lines model is effective and has been successfully used widely in the research field of *d* and *f*-elements single-molecule magnets.⁴²

For complex **MDAF-4Dy**, we only consider the nearest interactions between Dy^{III} ions.

The Ising exchange Hamiltonians for **MDAF-4Dy** is:

$$\hat{H}_{exch} = -J_1(\hat{\mathcal{S}}_{Dy1}^z \hat{\mathcal{S}}_{Dy2}^z + \hat{\mathcal{S}}_{Dy1}^x \hat{\mathcal{S}}_{Dy2}^x) - J_2(\hat{\mathcal{S}}_{Dy1}^y \hat{\mathcal{S}}_{Dy2}^y) \quad (1)$$

The $\tilde{J}_1 = 25 \cos \varphi J_1$, where φ is the angle between the anisotropy axis on two Dy^{III} sites, and J_1 is the Lines exchange coupling parameter. The \tilde{J}_2 also have similar expression.

The $\mathcal{S}_{Dy} = 1/2$ is the ground pseudospin on the Dy^{III} site. The total \tilde{J}_{total} is the parameter of the total magnetic interaction ($\tilde{J}_{total} = \tilde{J}_{dipolar} + \tilde{J}_{exchange}$) between magnetic center ions. The dipolar magnetic couplings can be calculated exactly, while the Lines exchange coupling constants were fitted through comparison of the computed and measured magnetic susceptibilities using the POLY_ANISO program.⁴⁰

Table S12. Exchange energies E (cm^{-1}), the energy difference between each exchange doublets Δ_t (cm^{-1}) and the main values of the g_z for the lowest eight exchange doublets of **MDAF-4Dy**.

	E	Δ_t	g_z
1	0.0	2.0×10^{-12}	0.000
2	0.5	1.6×10^{-7}	39.001
3	0.5	1.6×10^{-7}	39.001
4	0.9	4.0×10^{-12}	0.000
5	2.2	1.0×10^{-12}	0.000
6	2.8	2.0×10^{-8}	0.000
7	2.8	2.0×10^{-8}	0.000
8	3.4	4.0×10^{-12}	78.002

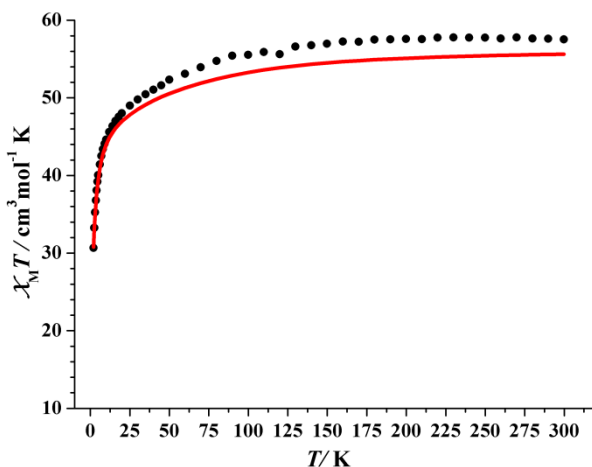


Figure S31. Calculated (red solid line) and experimental (black circle dot) data of magnetic susceptibilities of **MDAF-4Dy**. The intermolecular interaction zJ' of **MDAF-4Dy** was fitted to 0.01 cm^{-1} .

References:

- [1] Z. Chen, B. Zhao, P. Cheng, X.-Q. Zhao, W. Shi and Y. Song, *Inorg. Chem.*, 2009, **48**, 3493–3495.
- [2] P.-F. Shi, B. Zhao, G. Xiong, Y.-L. Hou and P. Cheng, *Chem. Commun.*, 2012, **48**, 8231–8233.
- [3] P.-F. Shi, G. Xiong, B. Zhao, Z.-Y. Zhang and P. Cheng, *Chem. Commun.*, 2013, **49**, 2338–2340.

- [4] Q. Zhou, F. Yang, B. Xin, G. Zeng, X. Zhou, K. Liu, D. Ma, G. Li, Z. Shi and S. Feng, *Chem. Commun.*, 2013, **49**, 8244–8246.
- [5] S. Mohapatra, B. Rajeswaran, A. Chakraborty, A. Sundaresan and T. K. Maji, Bimodal MagnetoLuminescent, *Chem. Mater.*, 2013, **25**, 1673–1679.
- [6] J. Baldoví, E. Coronado, A. Gaita-Arino, C. Gamer, M. GimenezMarques and G. M. Espallargas, *Chem. – Eur. J.*, 2014, **20**, 10695–10702.
- [7] Y.-X. Ren, X.-J. Zheng, L.-C. Li, D.-Q. Yuan, M. An and L.-P. Jin, *Inorg. Chem.*, 2014, **53**, 12234–12236.
- [8] M. Chen, E. C. Sañudo, E. Jiménez, S.-M. Fang, C.-S. Liu and M. Du, *Inorg. Chem.*, 2014, **53**, 6708–6714.
- [9] Q. Y. Liu, Y. L. Li, Y. L. Wang, C. M. Liu, L. W. Ding and Y. Liu, *CrystEngComm*, 2014, **16**, 486–491.
- [10] X.-J. Zhang, K. Liu, Y.-M. Bing, N. Xu, W. Shi and P. Cheng, *Dalton Trans.*, 2015, **44**, 7757–7760.
- [11] K. Liu, H. Li, X. Zhang, W. Shi and P. Cheng, *Inorg. Chem.*, 2015, **54**, 10224–10231.
- [12] X. Zhang, V. Vieru, X. Feng, J.-L. Liu, Z. Zhang, B. Na, W. Shi, B.-W. Wang, A. K. Powell, L. F. Chibotaru, S. Gao, P. Cheng and J. R. Long, *Angew. Chem., Int. Ed.*, 2015, **54**, 9861–9865.
- [13] C. M. Liu, D. Q. Zhang and D. B. Zhu, *RSC Adv.*, 2015, **5**, 63186–63192.
- [14] X. H. Yi, G. Calvez, C. Daiguebonne, O. Guillou and K. Bernot, *Inorg. Chem.*, 2015, **54**, 5213–5219.
- [15] A. J. Calahorro, I. Oyarzabal, B. Fernández, J. M. Seco, T. Tian, D. Fairen-Jimenez and E. Colacio, *Dalton Trans.*, 2016, **45**, 591.
- [16] I. Oyarzabal, B. Fernández, J. peda, S. Gómez-Ruiz, A.J. Calahorro, J. M. Seco and A. RodríguezDiéguez, *CrystEngComm*, 2016, **18**, 3055–3063.
- [17] J. M. Seco, I. Oyarzabal, S. Perez-Yerez, J. Cepeda and A. Rodríguez-Diéguex, *Inorg. Chem.*, 2016, **55**, 11230–11248.
- [18] C.-M. Liu, D.-Q. Zhang and D.-B. Zhu, *Chem. Commun.*, 2016, **52**, 4804–4807.
- [19] C.-M. Liu, D.-Q. Zhang, Y.-S. Zhao, X. Hao and D.-B. Zhu, *Inorg. Chem. Front.*, 2016, **3**, 1076–1081.
- [20] S. Wang, T. Cao, H. Yan, Y. Li, J. Lu, R. Ma, D. Li, J. Dou and J. Bai, *Inorg. Chem.*, 2016, **55**, 5139–5151.
- [21] R.-C. Gao, F.-S. Guo, N.-N. Bai, Y.-L. Wu, F. Yang, J.-Y. Liang, Z.-J. Li and Y.-Y. Wang, *Inorg. Chem.*, 2016, **55**, 11323–11330.
- [22] H. Iwami, R. Nakanishi, Y. Horii, K. Katoh, B. K. Breedlove and M. Yamashita, *Materials*, 2017, **10**, 81.
- [23] G. Huang, G. Fernandez-Garcia, I. Badiane, M. Camarra, S. Freslon, O. Guillou, C. Daiguebonne, F. Totti, O. Cador, T. Guizouarn, B. Le Guennic and K. Bernot, *Chem. Eur. J.*, 2018, **24**, 6983–6991.
- [24] J. Castells-Gil, J. J. Baldoví, C. Martí-Gastaldo and G. M. Espallargas, *Dalton Trans.*, 2018, **47**, 14734–14740.
- [25] F. Ma, J. Xiong, Y.-S. Meng, J. Yang, H.-L. Sun and S. Gao, *Inorg. Chem. Front.*, 2018, **5**, 2875–2884.

- [26] J.-W. Zhang, Y.-N. Ren, J.-X. Li, B.-Q. Liu and Y.-P. Dong, *Eur. J. Inorg. Chem.*, 2018, **2018**, 1099–1106.
- [27] X.-J. Zhang, F.-Z. Su, W.-Y. Guo, E. C. Sañudo and C.-S Liu, *Eur. J. Inorg. Chem.*, 2018, **2018**, 5007–5011.
- [28] L.-L. Luo, X.-L. Qu, Z. Li, X. Li and H.-L. Sun, *Dalton Trans.*, 2018, **47**, 925–934.
- [29] T. Hu, Q. Zhao, L. Huo, L. Gao, J. Zhang, X. Wang and L. Fan, *CrystEngComm*, 2018, **20**, 4291–4296.
- [30] Y. Xin, J. Wang, M. Zychowicz, J. J. Zakrzewski, K. Nakabayashi, B. Sieklucka, S. Chorazy and S. I. Ohkoshi, *J. Am. Chem. Soc.*, 2019, **141**, 18211–18220.
- [31] L. Zhang, S. Guan, Y. Fan, C. Du, D. Zhao and B. Liu, *Z. Kristallogr. – Cryst. Mater.*, 2019, **234**, 33–41.
- [32] C. Bai, C.-T. Li, H.-M. Hu, B. Liu, J.-D. Li and G. Xue, *Dalton Trans.*, 2019, **48**, 814–817.
- [33] L. H. G. Kalinke, D. Cangussu, M. Mon, R. Bruno, E. Tiburcio, F. Lloret, D. Armentano, E. Pardo and J. Ferrando-Soria, *Inorg. Chem.*, 2019, **58**, 14498–14506.
- [34] F. Ma, R. Sun, A.-H. Sun, J. Xiong, H.-L. Sun and S. Gao, *Inorg. Chem. Front.*, 2020, **7**, 930–938.
- [35] A. A. García-Valdivia, A. Zubala-Lekuona, A. Goñi-Cárdenasa, B. Fernándezc, J. A. Garcíad, J. F. Q. del Morale, J. Cepedab, A. Rodríguez-Diéguet, *Inorg. Chim. Acta*, 2020, **509**, 119687.
- [36] C. Zhang, X. Ma, P. Cen, X. Jin, J. Yang, Y.-Q. Zhang, J. Ferrando-Soria, E. Pardo and X. Liu, *Dalton Trans.*, 2020, **49**, 14123–14132.
- [37] T.-H. Yang, S.-F. Wang, C.-L. Lin, X. Wang, B. Zhua and D. Wu, *Dalton Trans.*, 2021, **50**, 1293–1299.
- [38] F. Aquilante, J. Autschbach, R. K. Carlson, L. F. Chibotaru, M. G. Delcey, L. D. Vico, I. F. Galván, N. Ferré, L. M. Frutos, L. Gagliardi, M. Garavelli, A. Giussani, C. E. Hoyer, G. Li Manni, H. Lischka, D. Ma, P. Å. Malmqvist, T. Müller, A. Nenov, M. Olivucci, T. B. Pedersen, D. Peng, F. Plasser, B. Pritchard, M. Reiher, I. Rivalta, I. Schapiro, J. Segarra-Martí, M. Stenrup, D. G. Truhlar, L. Ungur, A. Valentini, S. Vancoillie, V. Veryazov, V. P. Vysotskiy, O. Weingart, F. Zapata and R. Lindh, *J. Comput. Chem.*, 2016, **37**, 506–541.
- [39] L. Seijo and Z. Barandiarán, *Computational Chemistry: Reviews of Current Trends*; World Scientific, Inc.: Singapore, 1999, 455.
- [40] (a) L. F. Chibotaru, L. Ungur and A. Soncini, *Angew. Chem., Int. Ed.*, 2008, **47**, 4126–4129. (b) L. Ungur, W. Van den Heuvel and L. F. Chibotaru, *New J. Chem.*, 2009, **33**, 1224–1230. (c) L. F. Chibotaru, L. Ungur, C. Aronica, H. Elmoll, G. Pilet and D. Luneau, *J. Am. Chem. Soc.*, 2008, **130**, 12445–12455.
- [41] M. E. Lines, *J. Chem. Phys.*, 1971, **55**, 2977–2984.
- [42] (a) K. C. Mondal, A. Sundt, Y. H. Lan, G. E. Kostakis, O. Waldmann, L. Ungur, L. F. Chibotaru, C. E. Anson and A. K. Powell, *Angew. Chem. Int. Ed.*, 2012, **51**, 7550–7554. (b) S. K. Langley, D. P. Wielechowski, V. Vieru, N. F. Chilton, B. Moubaraki, B. F. Abrahams, L. F. Chibotaru and K. S. Murray, *Angew. Chem. Int. Ed.*, 2013, **52**, 12014–12019.